VYSOKÉ UČENÍ TECHNICKÉ V BRNĚ

Fakulta strojního inženýrství

DIPLOMOVÁ PRÁCE

Brno, 2017 Bc. Martin Čalkovský

VYSOKÉ UČENÍ TECHNICKÉ V BRNĚ
BRNO UNIVERSITY OF TECHNOLOGY

FAKULTA STROJNÍHO INŽENÝRSTVÍ
FACULTY OF MECHANICAL ENGINEERING

ÚSTAV FYZIKÁLNÍHO INŽENÝRSTVÍ
INSTITUTE OF PHYSICAL ENGINEERING

DEPOZICE GA A GAN NANOSTRUKTUR S KOVOVÝM JÁDREM
THE DEPOSITION OF GA AND GAN NANOSTRUCTURES WITH METAL CORE

DIPLOMOVÁ PRÁCE
MASTER'S THESIS

AUTOR PRÁCE — **Bc. Martin Čalkovský**
AUTHOR

VEDOUCÍ PRÁCE — **Ing. Jindřich Mach, Ph.D.**
SUPERVISOR

BRNO 2017

VYSOKÉ UČENÍ TECHNICKÉ V BRNĚ
FAKULTA STROJNÍHO INŽENÝRSTVÍ

Zadání diplomové práce

Ústav:	Ústav fyzikálního inženýrství
Student:	**Bc. Martin Čalkovský**
Studijní program:	Aplikované vědy v inženýrství
Studijní obor:	Fyzikální inženýrství a nanotechnologie
Vedoucí práce:	**Ing. Jindřich Mach, Ph.D.**
Akademický rok:	2016/17

Ředitel ústavu Vám v souladu se zákonem č.111/1998 o vysokých školách a se Studijním a zkušebním řádem VUT v Brně určuje následující téma diplomové práce:

Depozice Ga a GaN nanostruktur s kovovým jádrem

Stručná charakteristika problematiky úkolu:

GaN je polovodič s přímím přechodem, který se jeví jako velmi perspektivní pro polovodičový průmysl. Tento materiál lze připravovat unikátní nízkoteplotní metodou, kdy spolu s atomárními svazky (Ga) interagují dusíkové ionty o nízké energii. Nízká teplota procesu umožňuje přípravu GaN nanostruktur s kovovým jádrem, což může vést ke zlepšení fotoelektrických vlastností.

Cíle diplomové práce:

1) Provedení rešeršní studie přípravy a fyzikálních vlastností GaN nanokrystalů.
2) Příprava užitím MBE galiových nanostruktur s kovovým jádrem (Ag, Au, Al,...).
3) Příprava GaN nanokrystalů s kovovým jádrem užitím metody MBE-IBAD za různých fyzikálních podmínek (teplota substrátu, energie iontů,...).
4) Charakterizace a měření základních fyzikálních vlastností připravených Ga a GaN nanostruktur.

Seznam literatury:

Reshchikov, M., Evaluation of GaN by photoluminescence measurement, Phys. Status Solidi C, vol: 88 (7) pp: 2136-2138, (2011).

Gerlach, J., Ivanov, T., Neumann, L., Hirsch, D., Rauschenbach, B., Epitaxial GaN films by hyperthermal ion-beam nitridation of Ga droplets, Journal of Appl. Phys., vol: 111 (11), 113521, (2012).

Li, S., Waag, A., GaN based nanorods for solid state lighting. J. Appl. Phys. 111, 071101 (2012).

ABSTRACT

The presented thesis deals with preparation of GaN nanocrystals with a metal core. In the theoretical part of the thesis GaN with its properties and applications is introduced. Further, some of the preparation methods of GaN are presented, mainly focusing on MBE growth. Deposition of metal NPs from colloidal solution and the state of the art approaches to enhance luminescence of GaN based structures is discussed. The experimental part follows three steps of preparation of GaN crystals with the Ag core. In the first step the Ag NPs are deposited on the Si(111) substrate. In the second step the Ga deposition process is optimized and in the third step the deposited Ga is transformed into GaN. After the Ga deposition the samples were analyzed by SEM/EDX and SAM/AES. The properties of prepared GaN crystals with the Ag core were studied by XPS, photoluminescence and Raman spectroscopy.

KEYWORDS

GaN, metal core, enhanced photoluminescence, SERS

ABSTRAKT

Tato diplomová práce se zabývá přípravou GaN nanokrystalů s kovovým jádrem. V teoretické části této práce je představen materiál GaN se svými vlastnostmi a aplikacemi. Dále jsou uvedeny některé metody přípravy GaN, přičemž metoda MBE je popsána podrobněji. Dále je popsána depozice kovových nanočástic z koloidního roztoku a nejnovější metody zesílení luminiscence GaN struktur. Experimentální část je rozdělena na tři části odpovídající postupu přípravy GaN krystalů s Ag jádrem. V prvním kroku jsou Ag nanočástice naneseny na Si(111) substrát. Ve druhém kroku je optimalizován proces depozice Ga a v posledním kroku je nadeponované Ga transformováno na GaN. Po depozici Ga byly vzorky analyzovány pomocí SEM/EDX a SAM/AES. Vlastnosti připravených GaN krystalů s Ag jádrem byly studovány metodou XPS, fotoluminiscenční spektroskopií a Ramanovou spektroskopií.

KLÍČOVÁ SLOVA

GaN, kovové jádro, zesílená fotoluminiscence, SERS

ČALKOVSKÝ, M.
The deposition of Ga and GaN nanostructures with the metal core: master's thesis. Brno: Brno University of Technology, Faculty of Mechanical Engineering, Ústav fyzikálního inženýrství, 2017. 57 . Supervised by Ing. Jinřich Mach, Ph.D.

DECLARATION

I declare that I have elaborated my master's thesis on the theme of "The deposition of Ga and GaN nanostructures with the metal core" independently, under the supervision of the master's thesis supervisor and with the use of technical literature and other sources of information which are all quoted in the thesis and detailed in the list of literature at the end of the thesis.

Brno ....

(author's signature)

Acknowledgement

I would like to express my gratitude to my supervisor Ing. Jinřich Mach, Ph.D. for his helpful and valuable advices. My sincere thanks also go to Ing. Martin Konečný for his help with photoluminescence and Raman spectroscopy measurements, to Ing. Pavel Procházka for overlaying my samples with graphene, to Ing. Petr Bábor, Ph.D. for introducing me to SAM/AES, and to Ing. Tomáš Pejchal for preparing Al NPs. Special thanks belong to FEI company, which is now part of the Thermo Fisher Scientific, for financial support and to CEITEC Nano Research Infrastructure for enabling us to use their devices. I also want to acknowledge the great help of my wife and the entire family.

Martin Čalkovský

CONTENTS

INTRODUCTION

Gallium nitride (GaN) has been a very important semiconductor material for more than 50 years. The properties of this material, such as direct and wide bandgap, high electron mobility, high thermal conductivity, high chemical stability, ... have attracted many scientists to think of application in optoelectronics, photonics, high-power electronics, and other fields. Probably the most well known application of GaN is a blue light emitting diode (LED) awarded by Nobel prize in 2014 [1]. LEDs in general benefit from their energy-efficiency, high reliability and durability, and also for not containing mercury.

Compared to other light sources in LEDs the electricity is directly converted into light particles resulting in a high energy-efficiency. The efficiency is constantly improving and in the last few years attempts have been made to increase the efficiency of LEDs by embedding metal nanoparticles to the vicinity of the active layer of the LED [2]. In such a system the energy coupling between the active region of LED and the localized surface plasmon excited on the metal nanoparticle result in dramatic increase of luminescence efficiency.

Up to now metal nanoparticles were always embedded into the vicinity of the active layer in a second step, after GaN structures were prepared. In our work we aim to change the order and prepare GaN crystals with metal core. We want to focus on the technological aspect. In the first step metal nanoparticles will be deposited and in the second step GaN cryslats will be grown over the nanoparticles by modified ion-beam assisted molecular beam epitaxy (IBA-MBE). This GaN growth method is done at a low substrate temperature $T_S \sim 290°C$, which we believe is low enough not to influence the shape and size of metal nanoparticles. Also within the aim of this work is measuring properties of prepared structures (photoluminescence, surface enhance raman spectroscopy, ...).

The text is divided into several chapters. The first two theoretical chapters give a short introduction to thin film growth, to the fundamental properties of GaN, GaN applications, and to GaN preparation methods. The third chapter deals with metal nanoparticles. The deposition and use of metal nanoparticles is discussed. In the last chapter the experimental work is presented. Preparation of GaN crystals with a metal core consist of three steps. In the first step the metal nanoparticles are deposited on the substrate. In the second step Ga is deposited on the substrate with metal nanoparticles and in the last step the deposited Ga is converted into GaN using a N_2^+ beam. All these steps are discussed in detail. The photoluminescence, x-ray photoelectron spectroscopy, and raman spectroscopy measurements of prepared structures are also presented in this chapter.

1 THIN FILMS

Thin film physics is a branch of science studying materials with thickness ranging from a nanometer to several micrometers. This field is steadily growing due to unique mechanical, optical, and electrical properties that the thin film exhibits with decreasing the film thickness and because thin films offer the potential for low-cost processing with minimal material usage. Another advantage is also capability of applications where low weight and mechanical flexibility are crucial. In today's life, thin films play an important role in many commercially available applications such as eyeglasses, microelectronics, drill bits and cutting tools, solar cells, mirrors, flat screens, windows, semiconductors, etc.

Thin film growth process is called a deposition. For manufacturing thin films, many techniques has been developed (Chemical Vapor Deposition - CVD, Atomic Layer Deposition - ALD, Chemical Solution Deposition - CSD, Pulsed Laser Deposition - PLD, or Molecular Beam Epitaxy - MBE). All these techniques can be divided into two groups depending on the way precursor species are transported to the substrate [3].

- **Physical deposition techniques** - A source of compound to be grown is heated to a high temperature. Vaporized particles create a thermal-energy beam (E = 0.1-1 eV)transporting particles through the vacuum reactor toward the sample without any chemical change [4].

- **Chemical deposition techniques** - Molecules containing elements of the thin film to be grown are transported through the vacuum chamber to the reaction zone near the substrate. In the reaction zone the molecules dissociate, or undergo some chemical reaction to form a reactants that participate in the thin film growth [4].

1.1 Epitaxial growth

Epitaxial growth is a physical deposition process widely used in semiconductor industry. The word *epitaxy* comes from the Greek "epi"-upon, and "taxis"-to arrange [5]. In other words, the deposited overlayer on a crystalline substrate overtakes the crystalline structure of the substrate. In general, two types of epitaxial growth processes can be distinguished: **Homoepitaxy** - The growing layer and the substrate are made of the same material. On the other hand, when the materials are different, the epitaxy is called **Heteroepitaxy**. The epitaxial growth requires

Ultra-High Vacuum conditions (UHV [1]) to obtain a sufficiently large mean free path of deposited particles and to keep the sample clean throughout the deposition. The relatively slow growing rate (1 nm/min) and UHV conditions provide good control over the quality of the grown film.

The lattice constants of the substrate and the grown layer are crucial parameters for epitaxial growth. In homoepitaxy the lattice constants are the same, see Figure 1.1 a). In heteroepitaxy, Figure 1.1 b) and c), the different lattice constants can cause strain and dislocations near the interface and further degrade the quality of grown film. Choosing a suitable substrate with small lattice constant mismatch is a key to high quality films [6].

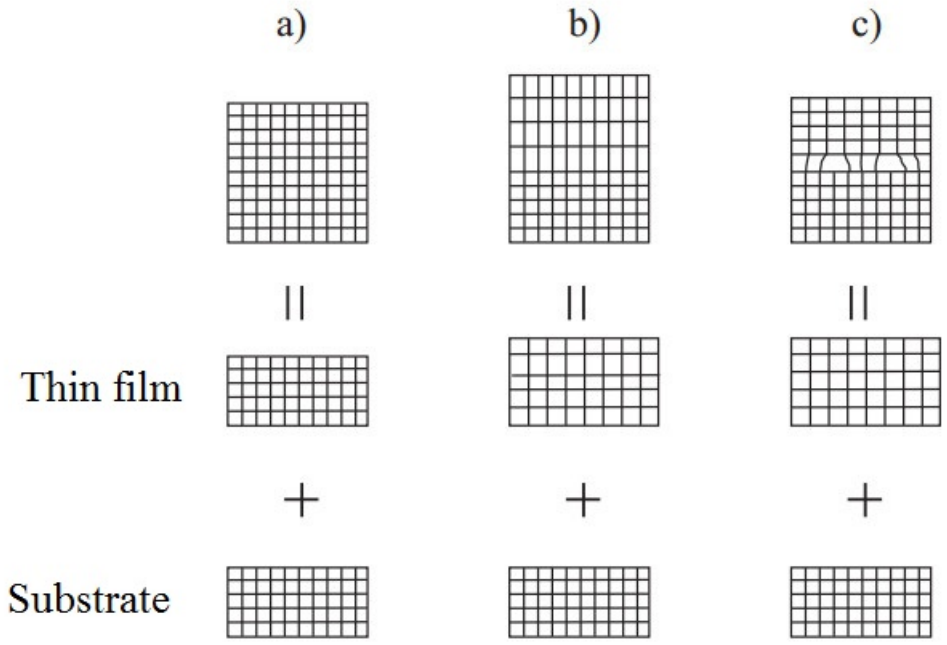

Figure 1.1: Schematically shown the influence of the lattice constant mismatch of a substrate and deposited thin film. a) The lattice constants are identical - homoepitaxy. Different lattice constants cause b) strain and c) dislocations near the interface. Adapted from ref. [6].

Impinging particle on the surface interacts with the surface and can be either reflected or adsorbed. The process is dependent on the incoming flux of atoms and on the sticking coefficient. An adsorbed atom, called adatom, lowers its potential energy and is physisorbed on the surface. In the physisorption process, the interaction between the adatom and surface is realized by weak Van der Waals forces. Physisorbed adatoms are relatively far from the surface and thus strongly mobile

[1] $p < 10^{-7}$ Pa

at room temperature (RT). Generally, at low temperatures the diffusion length increases with temperature, but at higher temperatures the desorption rate increases and overtakes the adsorption. Diffusing adatom can create a stronger chemical bond (charge transfer is present) with the surface - chemisorb [3, 7].

Thin film growth can occur in three characteristic modes (depicted in Figure 1.2) depending on forces between the growth constituents [8]:

- **Frank-van der Merwe (layer-by-layer)** - The force between adatom and the surface is stronger than the force between adatom and adatom. The result is a smooth layer, Figure 1.2 a).

- **Volmer-Weber (island formation)** - The force between adatom and adatom is stronger than the force between adatom and the surface. As a result islands are created on the surface, Figure 1.2 b).

- **Stranski-Krastanov (layer plus island)** - The growth in this mode is firstly dominated by layer-by-layer growth and then after overcoming a certain layer thickness the island growth is preferred, Figure 1.2 c). The critical thickness depends on surface energies and lattice parameters.

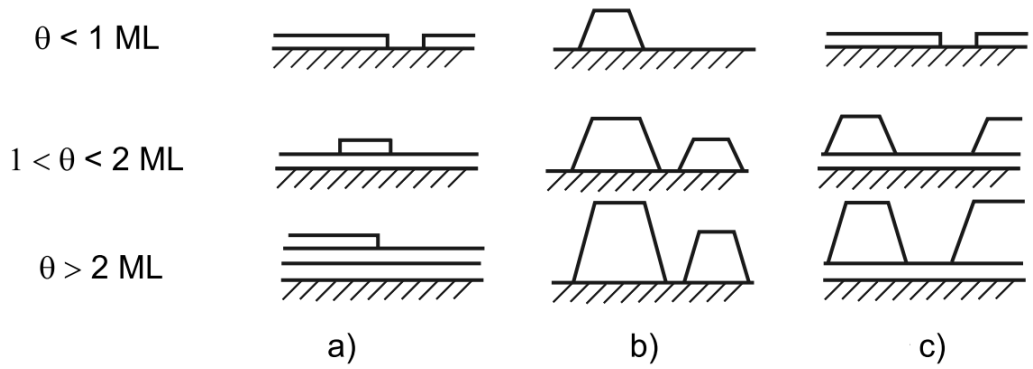

Figure 1.2: Thin film growth modes: a) Frank-van der Merwe (layer-by-layer) mode, b) Volmer-Weber (island formation) mode, and c) Stranski-Krastanov (layer plus island) mode. The parameter θ represents the number of monolayers. Adapted from ref. [8].

2 GALLIUM NITRIDE

Gallium nitride is a binary III/V semiconductor with direct bandgap of $E_g = 3.39$ eV at 300 K [9]. This compound is an assembly of N atoms and much larger Ga atoms crystallizing in three different crystallographic structures: hexagonal wurtzite structure, cubic zincblende, and cubic rocksalt structure. The most thermodynamically stable and thus the most studied and used is the hexagonal wurtzite structure.

The wurtzite structure shown in Figure 2.1 a) can be described as two hexagonal lattices (one of each atom kind - Ga and N) inserted into each other and shifted along $[000\bar{1}]$ direction by $3/8c$. Lattice constants a and c are ideally related as $c/a = \sqrt{8/3} = 1.633$.

Among the elements in the V$^{\text{th}}$ group, N has the highest electronegativity ($\chi = 3.04$). This high difference in electronegativity between N and metal elements in the III$^{\text{rd}}$ group [1] leads in a strong ionic behaviour of the covalent bond. As a result there are pairs of cation and anion atoms, along the [0001] direction, which are attracted to each other by electrostatic force. Therefore, most of the wurtzite crystals ratio c/a is smaller than the ideal value. For GaN the $c/a = 1.626$. It is considered that the decrease of c/a ratio make the wurtzite structure stabler than the zincblende structure [10].

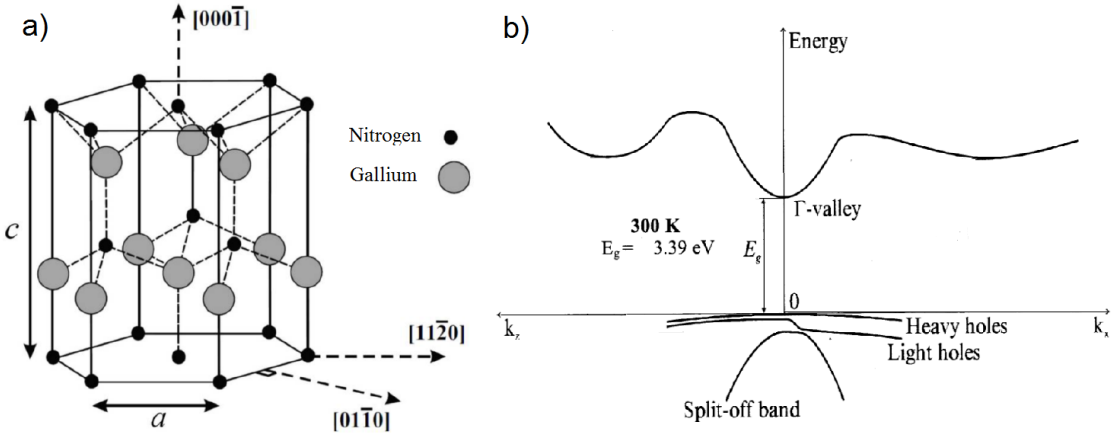

Figure 2.1: a) A schema of the hexagonal wurtzite crystal structure of GaN; a and c are lattice constants. Adapted form ref. [11]. b) Band structure diagram of the hexagonal wurtzite crystal structure of GaN. This structure exhibits a direct bandgap of $E_g = 3.39$ eV at 300 K. Adapted from ref. [12].

It was reported that cubic (zincblende) GaN single crystal thin film is possible to prepare using a modified molecular beam epitaxy technique [13]. Cubic GaN has the

[1] Electronegativity: 2.04, 1.61, 1.81, 1.78, and 2.04 for B, Al, Ga, In, and Tl, respectively [9].

Table 2.1: Properties of wurtzite GaN.

Property	**Value**	**Reference**
Energy band gap E_g (eV) at 300 K	3.4	[9]
Energy band gap E_g (eV) at 5 K	3.5	[14]
Density ($g \cdot cm^{-3}$)	6.15	[14]
Lattice constant a (nm)	0.318843	[15]
Lattice constant c (nm)	0.518524	[15]
Melting point (K)	> 2573 (at 60 kbar)	[15]
Maximum electron mobility ($cm^2 \cdot V^{-1} \cdot s^{-1}$) at 300 K	1350	[15]
Maximum electron mobility ($cm^2 \cdot V^{-1} \cdot s^{-1}$) at 77 K	19200	[15]
thermal conductivity ($W \cdot cm^{-1} \cdot K^{-1}$) at 300 K	2.1	[15]
Heat capacity ($J \cdot mol^{-1} \cdot K^{-1}$) at 300 K	35.3	[15]
Thermal expansion $\Delta a/a$ (K^{-1})	5.59×10^{-6}	[14]
Thermal expansion $\Delta c/c$ (K^{-1})	3.17×10^{-6}	[14]

potential for a higher saturated electron drift velocity and somewhat lower band gap. These properties could increase its applicability for high-frequency devices as well as short-wavelength light emitting diodes and semiconductor lasers, but preparing stable cubic GaN crystals is still difficult.

2.0.1 Properties of GaN

GaN has become one of the most important semiconductors not only for its direct and wide bandgap (Figure 2.2 b)) but also for high electron mobility, high thermal conductivity, high saturated electron drift velocity, etc [16]. Some basic properties of wurtzite GaN are summarized in Table 2.1. Beyond the properties listed in the table, GaN is an attractive material for its high chemical stability at elevated temperatures (up to 1173 K) and its suitability for caustic environment [14].

High dielectric strength, high electron mobility, and large electron drift velocity of GaN play a key role in current electronic technologies [17]. Dielectric strength of GaN is ~ 10 times higher than exhibit Si or GaAs, enabling the construction of electronic components working with much higher voltages and currents. The electron mobility of GaN does not reach extremely high values[2] due to relatively

[2]For comparison, electron mobility in InN is 3200 $cm^2 \cdot V^{-1} \cdot s^{-1}$ at 300 K [14].

high effective electron mass (m = 0.2 m_e).[3] Another feature restricting the electron mobility is scattering on the impurities and dislocations, or at high temperatures the scattering on phonons [18].

GaN form solid solutions with AlN and InN, making a wide range (1.9-6.2 eV) of energy band gaps possible. This ability to form alloys is essential for producing specific wavelengths for emitters, and for creating heterojunctions with potential barriers into the device structures [15]. Band structure of wurtzite GaN is shown in Figure 2.1 b). The splitting of the valence band results from spin-orbit interactions and from crystal symmetry [12]. According to Bougrov *et al.* [19], temperature dependence of the bandgap is given by the following relation

$$E_g(T) = E_g(0) - 7.7 \times 10^{-4} \frac{T^2}{T + 600} (\text{eV}), \tag{2.1}$$

where T is temperature in K and $E_g(0) = 3.47$ eV and $E_g(0) = 3.28$ eV for wurtzite and zincblende structure, respectively. Parameters such as band gap E_g, dielectric constant ε, melting temperature T_m, and Young's modulus Y are treated as a constant for a bulk specimen and they are almost not correlated. However, at the nanoscale these parameters become tunable due to the size and shape dependences, and the change trends with size and shape are different from one another. Numerous computer simulations and experimental studies have found that the E_g increase while the T_m, Y, and ε decrease with the decreasing size [21].

2.0.2 GaN Applications

Only in recent years successful development of methods for growing a high quality GaN on top of standardized Si wafers have been invented. Because of that, GaN wafers can be produced in the same factory that silicon wafers are produced, and therefore their price has decreased dramatically. Properties of GaN promise to replace the silicon predominance in current semiconductor technology.

Potential and current use of GaN technology are as follows:

- **White or color light emitting diodes (LEDs)**. In early 1990s Isamu Akasaki, Hiroshi Amano and Shuji Nakamura produced the first bright blue light beams from semi-conductors. Their invention was awarded with the Nobel Prize in Physics in 2014, and started the Light revolution. LEDs benefit form high reliability, high durability (up to 100 000 hours), and low energy consumption. The LEDs are constantly improved, getting more efficient. The

[3] For comparison, effective electron mass at 300 K in GaAs and InN is m = 0.06 m_e and m = 0.11 m_e a, respectively [20].

most recent record in efficiency is just over 300 lumen·watt^{-1}, which can be compared to 16 regular light bulbs. Today GaN-based LEDs provide the dominant technology for back-illuminated liquid crystal displays in many mobile phones, tablets, laptops, computer monitors, TV screens, etc. Future application may include the use of UV-emitting AlGaN/GaN LEDs for water purification, as UV light destroys the DNA of bacteria, viruses and microorganisms [1].

- **Blue and violet laser diodes (LDs)**. Laser diodes based on GaN have caused a revolution in communications and in optical data storage. They also offer a chance to extend diod laser spectroscopy to blue region of the spectrum [22].
- **High power-high frequency transistors**. Power converters are constantly trending towards higher output power, higher efficiency, higher power density, higher temperature operation, and higher reliability. The GaN HEMT transistors demonstrated superior performance comparing to Si-based power devices, driving the next wave of power electronics revolution [23].

2.1 Substrates for the growth of GaN

For semiconductor growth homo-epitaxy is the best for producing high quality semiconductor films. Even though GaN single crystal can be prepared, the small size and high price prevents it from becoming commercially available. Therefore the heteroepitaxy process is usually used in GaN growth. There are many substrates (including insulating metal oxides, metals, metal nitrides, and other semiconductors) for GaN growth that have so far been reported [15]. The most important criteria for choosing a suitable substrate is the lattice constant mismatch because it incorporates strain into the epitaxial layer. The resulting properties of the epitaxial layer are greatly influenced not just by the lattice constant mismatch, but also by the crystal structure, surface finish, composition, reactivity, chemical, thermal, and electrical properties of the substrate. Table 2.2 shows the most used substrates with their basic parameters.

Choosing a suitable substrate plays a key role in the quality, and thus in the applicability of the grown GaN. On the other hand it has been found that the emission efficiency of the GaN based LEDs was not influenced by the dislocation density [24].

2.1.1 Sapphire (Al_2O_3)

Sapphire (Al_2O_3) has been the most widely used substrate material for the growth of GaN because of its good optical quality, thermal stability, availability of large

Table 2.2: Substrate candidates for GaN growth and their parameters. Adapted from ref. [15, 24].

Material	**Structure**	**Latice mismatch (%)**	**Lattice constant (Å)**	
			a	c
GaN	Wurtzite	0	3.19	5.19
Al_2O_3	Rhombohedral	~ 15	4.77	12.98
SiC (6H)	Wurtzite	$\sim$3.5	3.09	15.12
Si	Diamond	$\sim$21	5.43	-
Ge	Diamond	~ 20	5.66	-
GaAs	Zincblende	$\sim$20	5.65	-
ZnO	Wurtzite	$\sim$1.8	3.25	5.21
GaP	Zincblende	$\sim$20	5.43	-

size, and low cost [14]. Contrary, the disadvantages of sapphire are large thermal expansion coefficient which produce biaxial compressive stress in the GaN layer as it cools from the deposition temperature.

The lattice mismatch between GaN and sapphire is relatively high $\sim 15\%$, leading to high dislocation density (10^{10} cm^{-2}) [15]. To minimize the lattice mismatch, instead of the most popular (0001) plane sapphire, several other planes have been studied. The most promising $(11\bar{2}0)$ plane, with mismatch only $\sim 2\%$, show bad quality of grown GaN because the difference in the planar symmetry results in highly strained bonds near the interface [25].

To obtain high quality GaN on either of sapphire plane, sapphire nitridation and low temperature GaN buffer layer procedures were introduced [25]. Firstly, the substrate surface is annealed under flowing air at 1400 °C to remove contaminants and to reduce the roughness of the surface after polishing. Secondly, the sapphire is nitridated by exposure to nitrogen plasma to reduce the defect density and to enhance the electron mobility. Lastly, a thin buffer layer of GaN (10-100 nm) is deposited at a low temperature and then annealed to improve the surface morphology. An epitaxial GaN film grown on such treated substrate is used in many current applications [15].

2.1.2 Silicon Carbide (SiC)

Among several crystal structure that SiC has, the 6H-SiC is the most widely used for GaN growth. 6H-SiC has several advantages over the sapphire, including smaller

lattice constant mismatch (3.5%) and much higher thermal and electrical conductivity. Because of these properties GaN grown on 6H-SiC is widely used for electronic devices [24]. Another advantage of SiC is its availability in both carbon and silicon polarities enabling control over the the polarity of GaN film.

However SiC does have its disadvantages. Beside substantial price the surface of commercially available SiC is fairly rough (RMS[4] roughness ∼1 nm). Such a roughness influences the deposited film and therefore it is important to prepare the surface prior deposition. Methods including etching in HCl + H_2, reactive ion etching, high temperature ($T \sim = 1600°C$) etching in hydrogen, or atomic hydrogen irradiation are usually used [24].

2.1.3 Silicon (Si)

Silicon (Si) is a very attractive material for GaN fabrication. Silicon wafers are very cheap due to a large scale production and the crystal quality of the Si wafers is excellent. The Si(111) substrate is usually preferred for GaN epitaxy due to the hexagonal-like arrangement of Si atoms on the (111) plane. The quality of GaN epitaxial layers on Si is much poorer than on sapphire or SiC, due to large lattice constant and thermal expansion coefficient mismatch, and the tendency of silicon to form an amorphous silicon nitride layer when exposed to reactive nitrogen sources. Nevertheless, many GaN devices have been fabricated on silicon substrates even though there is usually a buffer layer needed [15].

2.1.4 Germanium (Ge)

Despite the substantial lattice constant mismatch between GaN(0001) and Ge(111) - 20 %, GaN growth on Ge(111) has been recently reported [26]. To overcome the lattice mismatch, formation of a few monolayers of crystalline Ge_3N_4 occurs just before the start of GaN growth. Such prepared GaN layers consist of misoriented domains. Suppression of the domain formation can be done by increasing the substrate temperature or by decreasing the nitrogen flux [27]. The main advantage of using Ge as a substrate for III-nitrides is relatively small thermal expansion coefficient mismatch ($\sim 5.5\%$) [26].

[4]Root Mean Square (RMS) is defined as the square root of the arithmetic mean of the squares of certain values.

2.2 Preparation methods of bulk and thin film GaN

Due to high covalency of GaN the decomposition pressure at the melting point is extremely high[5]. For this reason the standard techniques of crystal growth generally used for the elaboration of semiconductor wafers (Bridgman, Czochralski, Verneuil) cannot be developed [28]. Even though methods for preparation of bulk GaN were developed, it is still difficult to prepare large and high quality crystals. Because of the lack of bulk GaN substrates, the currently available devices use GaN thin films prepared by methods listed below on different substrates (heteroepitaxy).

2.2.1 High Pressure Nitrogen Solution growth (HNPS) and Sodium-flux method

The High Pressure Nitrogen Solution (HNPS) growth method is based on a direct reaction between liquid gallium and gaseous nitrogen at high temperature (up to 1800 K) and high nitrogen pressure (up to 1 GPa). The growth mechanism of HPNS is as follows: Nitrogen molecules dissociate on gallium surface and dissolve in the metal. The driving force of the crystallization process is created by the application of a temperature gradient along the liquid gallium. Due to this gradient, atomic nitrogen is transported from the hot end of the solution to the cooler part, where the GaN crystallizes and grows [29]. Schematic illustration of the crystallization process is in Figure 2.2 a). HNPS method grows very high-quality GaN crystals with dislocation density less than 2×10^2 cm^{-2}. The main drawback is a very slow growth rate enabling a crystal size of only several millimeters [16].

Sodium (Na)-flux method is an improved HNPS method. The main improvement is adding Na into Ga melt. Atoms of Na act as a catalyst for the dissociation of N_2 molecules, enabling great decrease of the growth temperature and pressure to values around $T = 850$°C and $p = 5$ MPa [30]. By adding a powdery carbon into the Ga melt, generation of polycrystals in markedly suppressed. The Na-flux method, with grow rate up to 10 μm·h^{-1}, lower pressure and temperature is expected to be used for mass production. Nevertheless, the growth rate must be improved to several times faster than the current value to be used for mass production techniques [31].

[5]The decomposition pressure at the melting point T $\sim$ 2500 °C is $\sim$ 4.5 GPa [28]. For pressures below the decomposition pressure the GaN does not melt and thus decomposes.

2.2.2 Hydride Vapor Phase Epitaxy (HVPE)

Hydride Vapor Phase Epitaxy (HVPE) has been introduced more than 40 years ago [32]. Since then a lot of effort has been devoted to bringing this method to be the most widely used in todays GaN growth.

Usually HVPE reactor (Figure 2.2 b)) consists of two or more reactive zones [33]. The first one is the source zone, where gaseous HCl react with liquid Ga at temperatures T = 750-900°C forming GaCl according to equation

$$2\mathrm{Ga} + 2\mathrm{HCl} \longleftrightarrow 2\mathrm{GaCl} + \mathrm{H_2}. \tag{2.2}$$

Afterwards the GaCl and NH_3 are transported to the second zone (deposition zone) separately by a carrier gas mixture of H_2 and inert gas. At the deposition zone, the source species are mixed and react at temperatures T = 900-1100°C to form GaN on the substrate according to equation

$$\mathrm{GaCl} + \mathrm{NH_3} \longleftrightarrow \mathrm{GaN} + \mathrm{HCl} + \mathrm{H_2}. \tag{2.3}$$

GaN grown by HVPE generally show n-type conductivity due to residual donor impurities such as O and Si, which may degrade device performance. Intentional doping is accomplished during the growth process by introducing the dopant (Fe, Cr, or Zn) to the growth apparatus, either as its hydride or by direct evaporation of the element into a hydrogen-carrier gas [32]. Fe-doping is widely used for its reproducibility and controllability. An Fe concentration above 10^{15} cm^{-3} is sufficient to compensate unintentionally incorporated donor impurities and native defects [16].

Hydride vapor phase epitaxy is a high-growth-rate technique capable of several hundred micrometers per hour growth rate. GaN can grow up to several millimeters, which is thick enough for the fabrication of bulk substrates.

2.2.3 Molecular Beam Epitaxy

Conventional Molecular Beam Epitaxy (MBE) has become one of the most important methods for preparation and study of GaN films because of the possibility to prepare high quality layers with sharp abrupt interfaces, good control of thickness, potential of manufacturing more complex semiconductor components, and the possibility to monitor the growth by *in situ* diagnostics [14].

In the MBE process in general the constituent elements of the semiconductor in the form of molecular beam are deposited onto a heated substrate to grow an epitaxial layer. The process of epitaxial growth was discussed in section 1.1. In case

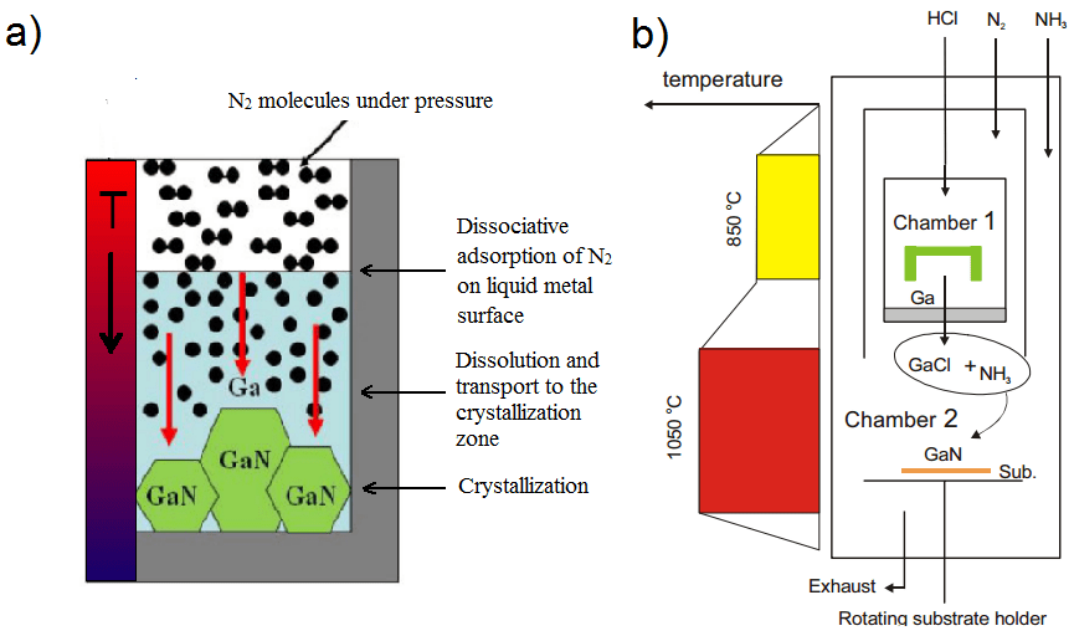

Figure 2.2: a) Schematic illustration of the crystallization process in a temperature gradient by the HNPS method. Adapted from ref. [29]. b) Schematic drawing of a HVPE reactor. It consists of two separate chambers: Chamber 1 is for the synthesis of the GaCl precursor, chamber 2 is for mixing the precursor GaCl and NH_3, and for GaN deposition. Adapted from ref. [11].

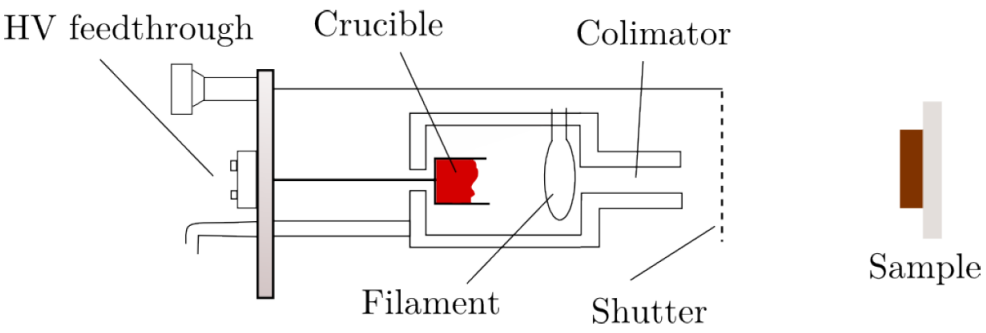

Figure 2.3: The Schema of the effusion cell used for Ga deposition. Adapted from ref. [34].

of GaN MBE growth the Ga beam is formed by an effusion cell, schematically described in Figure 2.3. Between the molybdenum crucible, filled with 99.9999% pure Ga, and the tungsten filament a voltage up to 1000 V is applied. The tungsten wire is heated by current to temperatures $T \sim 2800$ K where the thermal electron emission occurs. The emitted electrons are accelerated towards the crucible. In this way the crucible, and thus the Ga inside, is heated to temperatures where sufficient Ga evaporation starts. Evaporated Ga atoms are passing through the collimator towards the substrate. The deposition rate is governed by the temperature of Ga in the crucible. A small portion of Ga atoms passing through the collimator are ionized and therefore current I_J can be measured, in nA range. The number of ionized Ga atoms is proportional to the number of neutral Ga atoms in the beam.

To grow GaN, a source of N particles is needed. The most widely used atomic N source is the radio frequency (RF) plasma source. In this source nitrogen plasma is generated by inductively coupling the RF energy at 13.56 MHz into a discharge chamber filled with nitrogen [35]. Even though different species of N are produced, the atomic N flux can reach high values. The flux of N atoms is accelerated toward the substrate by the pressure gradient with the vacuum chamber. N atoms arrive to the surface with low energy of $E \sim 1$ eV which allow reaction with Ga to form GaN [36].

In our laboratory at the Institute of Physical Engineering we use electron-impact ion source producing N_2^+ ions [37]. This ion source is schematically shown in Figure 2.4. The principle of such an ion source is as follows: The thermal electrons emitted from a tungsten filament (cathode) are accelerated towards the ionization grid (anode). N_2 molecules are brought in the inner part of the ion source by a UHV leak valve and ionized by collisions with accelerated electrons, creating N_2^+ ions. The energy of N_2^+ ions reaching the surface in $E = 50$ eV, which is sufficient to dissociate[6] on the surface and make a bond with the Ga atom to form a GaN.

The method described above is known as ion-beam assisted MBE (IBA-MBE). There are several advantages of this method: direct mass and energy control of the ion beam and its incidence angle, UHV conditions making in-situ analysis possible and an energy excess of ions compared to average atom energies in evaporation methods [40].

In our experiments we have used a modified (IBA-MBE) method know as droplet epitaxy [41]. The difference is in separating the Ga deposition from the reaction of Ga with reactive nitrogen species, i.e., Ga is deposited first and afterwards post-nitridation of Ga takes place. This approach is capable of manufacturing high

[6]The dissociation energy of N_2 molecule is $E = 9.76$ eV [38].

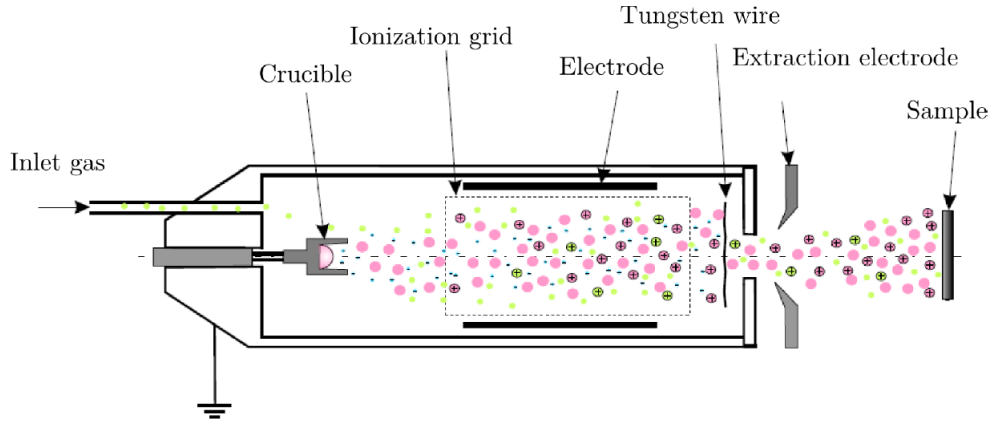

Figure 2.4: The schematics of electron-impact nitrogen ion source. Adapted from ref. [39].

crystalline quality GaN thin films as well as high quality GaN nanocrystals [41].

The theory behind the transformation of Ga droplets into an epitaxial GaN film was proposed by *Gerlach et al.* [41].The process is schematically described in Figure 2.5. The initial state (after the 1st step in growth process) is shown in Figure 2.5 a). The deposited Ga atoms form a stable liquid Ga droplets on the surface. In the second deposition step, the hyperthermal ($E < 25$ eV) N_2^+ ion beam is applied on the surface. The deposited nitrogen diffuse on the surface of the liquid gallium droplet to peripheral regions of the liquid-solid interface (Figure 2.5 b)). The main driving force for this diffusion is the decrease in the surface energy. Further, at the peripheral region the liquid-solid interfacial diffusion and crystallization towards the center occurs (Figure 2.5 c)). In the final state GaN islands are formed (Figure 2.5 d)).

2.3 Preparation of GaN nanostructures

GaN nanostructures have many potential advantages as compared to 2D GaN thin films. Namely that GaN nanorods are emerging as a very promising novel route toward devices for nano-optoelectronics and nano-photonics. Growth processes of GaN nanorods can be divided into two groups; catalyst-assisted and catalyst-free growth.

2.3.1 Catalyst-assisted GaN nanorod growth

Among the catalyst-assisted growth methods, vapor-liquid-solid (VLS) growth mechanism is mostly used. As a catalyst for GaN nanorods, Au, Ni, or Pt is often used. The growth process of VLS is schematically described in Figure 2.6 a). In the first

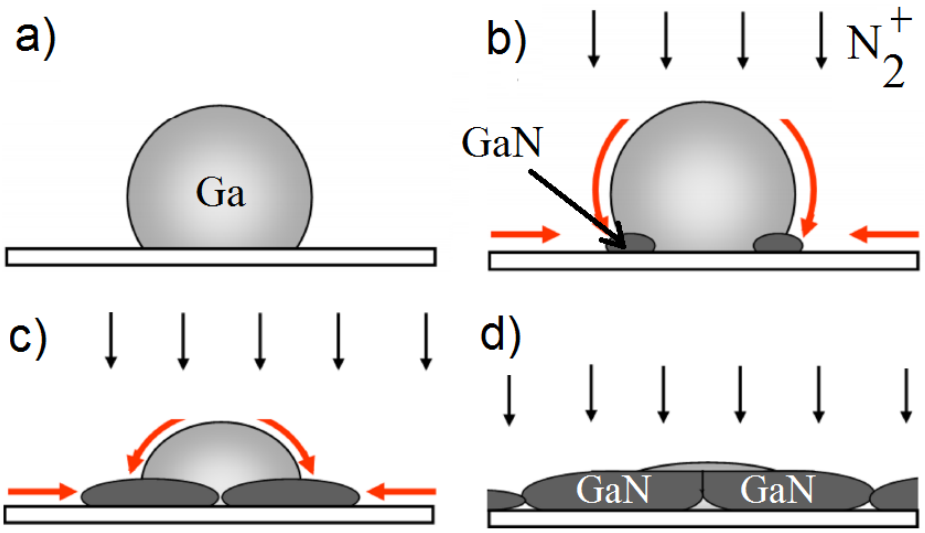

Figure 2.5: Schematics of transformation of Ga droplets into a GaN by low energy nitrogen ion irradiation. a) Ga liquid droplets on the surface. b) Nitrogen ions are diffusion along the Ga surface to the peripheral region where crystallization occurs. c) Further GaN growth. d) Final state of prepared GaN. Adapted from ref. [41].

step, catalytic nanoparticles are deposited on the substrate. In the next step, Ga and N atoms are deposited on the surface. They diffuse to the interface of the catalyst and substrate where GaN crystallizes. In this way the catalyst NP is lifted by the growing GaN nanorod. The growth occurs only on the catalyst NP interface and therefore a GaN nanorod mostly perpendicular to the surface is formed [42]. Oh *et al.* [43] reported a GaN nanorods with diameter $\sim$ 100 nm and lengths of $\sim$ 5 μm. An SEM image of GaN nanorods grown from Au NPs is shown in Figure 2.6 b).

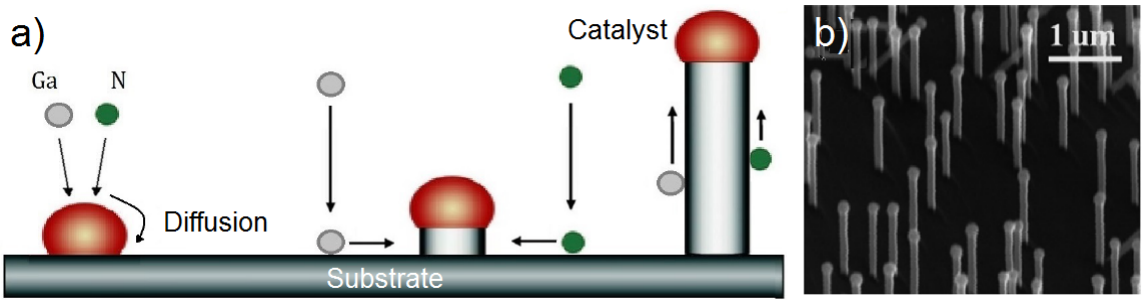

Figure 2.6: a) Schematics of GaN nanorod catalyst-assisted VLS growth. Adapted from ref. [44]. b) SEM image of the GaN nanorods grown from Au NPs. Au NPs can be seen on top of GaN nanorods. Adapted from ref. [45].

The catalyst plays a key role in the VLS growth process and also affects the optical properties of the prepared structure. Li *et al.* [45] studied the VLS growth process using Ni catalyst. They found Ni contamination and basal-plane stacking faults resulting in a decreased photoluminescence intensity. For this reason GaN nanorods grown with catalyst may not be well suitable for LED applications. The advantage of catalyst-assisted growth of nanorods is a relatively large growth rate [45].

2.3.2 Catalyst-free GaN nanorod growth

The presence of catalyst in the GaN nanorod growth induces some imperfections, and therefore catalyst-free growth is needed for some applications. GaN nanorods can be grown without the catalyst by MBE and MOCVD methods, even though the exact principle of the growth is still under debate. It was found by many groups that the V/III ration is a crucial factor for MBE growth. High V/III ration means N-rich conditions where the diffusion length of Ga atoms is reduced, resulting in reducing the coalescence of the nucleation sites. High V/III ration leads to GaN nanorod growth, while low V/III ration enables a layer growth [45].

GaN nanorods can be grown on a bare substrate (Si, sapphire, ...) but usually for high quality an AlN buffer layer is needed. The thickness of this AlN layer is very important for successive GaN nanorod growth. With increased AlN thickness the density of GaN nanorods dramatically increases. The nucleation mechanism is also closely related to AlN layer. It was found that the edge facets of AlN grains provide crystal nucleation sites [45].

One of the growth mechanisms, diffusion-induced mechanism, was explained by Debnath *et al.* [46]. In this model the adatoms diffuse to the wire apex from its lateral sides driven by a lower chemical potential at the top surface. This diffusion process contributes to the nanorod growth in addition to the direct impingement of the atoms at the tip of the nanorod. This process is schematically shown in Figure 2.7 a). The nucleation rate of the nanorods is strongly dependent on the density of nanorods and at certain nanorod density drops to zero. After nucleation, the diameter of the nanorods grow slower compare to the length resulting in the formation of nanorods with large length/diameter ration. GaN nanorods prepared within this method are shown in Figure 2.7 b).

Another catalyst-free growth model is in analogy to the catalyst-assisted VLS growth [48]. Here the Ga droplets play the role of catalyst, therefore this model is also called self-catalyzed VLS growth. Unfortunately, the residual Ga droplets has never been observed on the nanorod tip in the N-rich conditions [49].

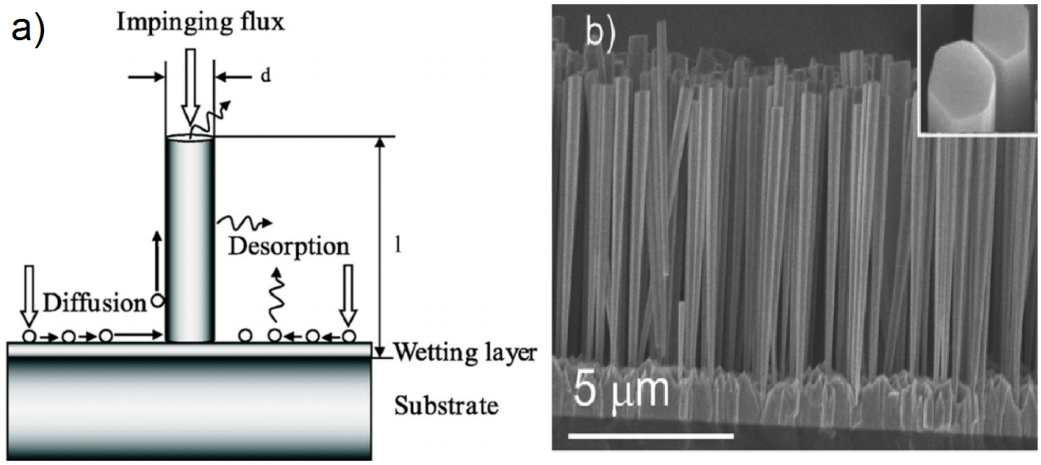

Figure 2.7: a) Schematics of the catalyst-free diffusion-induced mechanism GaN nanorods growth. Adapted from ref. [46]. b) SEM image of such prepared GaN nanorods. Adapted from ref. [47].

The catalyst-free GaN nanorod growth is a very promising for further optoelectronic applications, and therefore a deeper understanding of the growth process is needed.

3 METAL NANOPARTICLES

Metal nanoparticles have been used for centuries by artists during glass coloring processes. Metallic nanoparticles were first reported in 1857 by Michael Faraday. He discovered that their optical properties are different from those of bulk metals [50]. Further studies have shown that reduction of bulk materials to nanosize dimensions dramatically change physical and chemical propertias of certain material. Metallic nanoparticles have huge potential in future nanotechnology. Nowadays they are heavily utilized in biomedical sciences and engineering focusing on plasmonics, surface enhanced raman spectroscopy, targeted drug delivery, diagnostic imaging, and others [51]. Many preparation methods have been made public, including both top-down and bottom-up approaches [52]. In this work we are interested mostly in silver nanoparticles (Ag NPs).

3.1 Deposition of silver nanoparticles

It was reported that silver nanoporticles (Ag NPs) can be prepared by laser ablation, gamma irradiation, electron irradiation, chemical reduction, photochemical methods, microwave processing, and biological synthetic methods [53]. Within some preparation methods, stabilization of the created Ag NPs is needed. This is done by stabilizing agents that cap the Ag NPs. Ag NPs prepared by different methods slightly differ in their properties (size, reactivity, ...). Because of the large demand for NPs in the scientific and engineering field, metal NPs became commercially available. Ag NPs with diameter varying in range 10 - 100 nm are sold by many companies (BBI, Sigma-Aldrich, Ted Pella, nanoComposix, mkNANO, ...). In the last few years, Ag NPs covered with a SiO_2 shell (Silica shelled Ag NPs) also became commercially available. Almost all Ag NPs are stored in colloidal solution. To prevent clustering of NPs in the colloidal solution, a stabilization agent is needed. This role in most cases play anion of citric acid - citrate. In Figure 3.1 a) transmition electron microscope image show atoms of metal (Au) surrounded by citrate molecules, forming a stabilized Au nanoparticle.

The amount of negative charge on a NP cannot be easily determined. Therefore in colloidal science the quantification of charge on a NP is defined by zeta potential which can be indirectly measured [56]. Zeta potential reflects the potential stability of the colloidal system. If all NPs show high positive or high negative zeta potential, then the NPs will repel each other - colloidal solution is stable. Colloidal solutions are usually considered unstable if their respective zeta potential value decreases below $\pm$ 30mV [57].

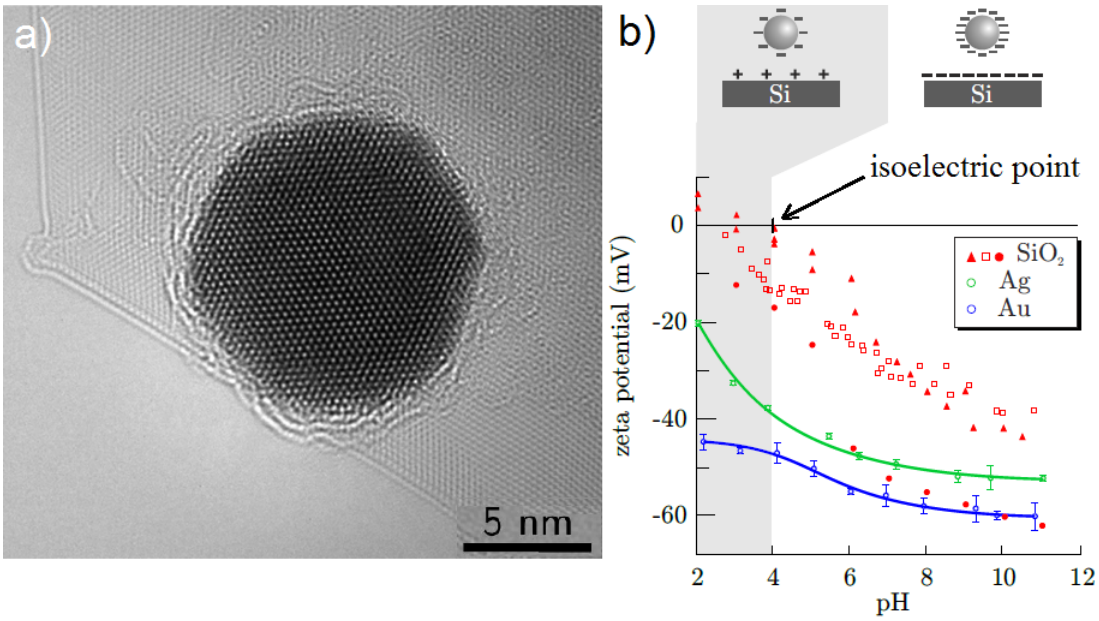

Figure 3.1: a) Transmition electron microscope image of 10 nm Au NP surrounded by citrate molecules. Adapted from ref. [54]. b) Zeta potential dependence of SiO_2, Ag a Au on the pH of the surrounding medium. The region of pH where deposition of Ag/Au NPs on the SiO_2 surface occurs is grayed out. Adapted from ref. [55].

Zeta potential strongly depends on pH of the surrounding medium [58]. Figure 3.1 b) shows zeta potential dependence on pH for Ag NPs, Au NPs, and for SiO_2 substrate. Zeta potential curve for SiO_2 reaches zero for pH = 4 (i.e. Isoelectric point) and for lower pH zeta potential is positive. This feature plays a key role in the deposition process, since there exists a region of pH where zeta potentials for metal NPs and for SiO_2 substrate have opposite signs, resulting in an attractive force between the metal NPs and SiO_2 substrate. The process of NPs deposition is shown in Figure 3.2 a), and is rather simple. The typical colloidal Ag/Au solution has a pH of 5.5 whereas the isoelectric point of conventional silicon wafers varies between pH of 3–4. To reach smaller pH, HF or HCl is added to the solution. By dipping the sample into such prepared solution, metal NPs are deposited on the surface. The density of deposited NPs is proportional to dipping time and inversely proportional pH [55]. Biggest drawbacks of this deposition method are surface contamination and random distribution of deposited NPs.

For many applications, randomly placed NPs are not suitable. For this reason selective deposition processes were developed. The procedure developed at the Institute of physical engineering in Brno requires only two steps. Si sample with native SiO_2 is exposed to a beam of charged particles (electrons or ions) and after that dipped into a NPs colloidal solution modified by HF. The electron (ion) beam

interacts with the surface and locally modifies its chemical properties and therefore also zeta potential changes. By tuning the parameters of an electron (ion) beam, selective deposition of metal NPs is possible [59]. The process is schematically shown in Figure 3.2 b).

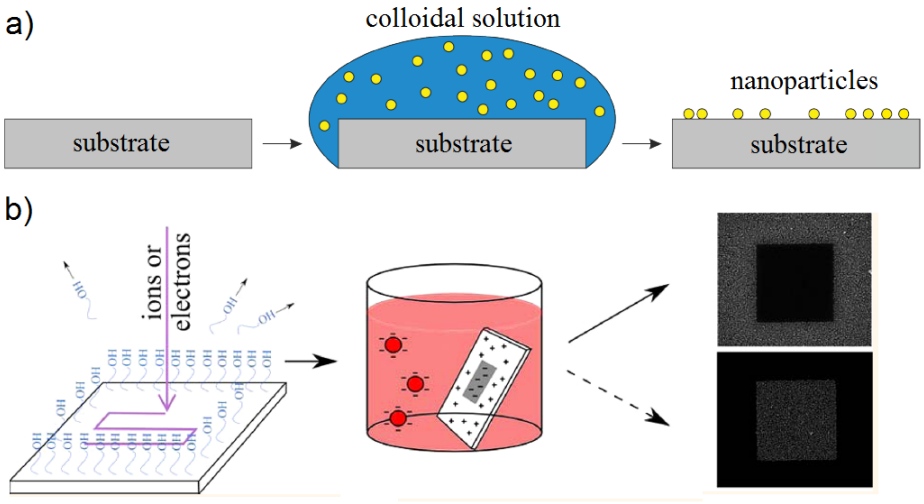

Figure 3.2: a) Schematics of Ag/Au NPs deposition from colloidal solution. Adapted from ref. [60]. b) Selective two step deposition process of Ag/Au NPs from colloidal solution. The sample is exposed to an electron beam and dipped into a colloidal solution modified by HF. Adapted from ref. [59].

3.2 Photoluminiscence (PL)

Luminescence (sometimes called fluorescence) is a general term for emission of light from a substance after or during the adsorption of excitation energy. Depending on how the excitation energy is supplied to the substance, different luminescent phenomena can be distinguished: *Photoluminescence* - is excited by photons, usually with energy of several eV. *Cathodoluminescence* - is excited by an electron beam with energy of 10^2 - 10^3 eV. *Electroluminescence* - excited by applied voltage and current passing through the substance [61].

It has to be noted that luminescence is not a thermal radiation or Raman and Compton effect. Luminescence can be easily distinguished from other physical effects because of the time delay in the luminescence emission after excitation, which is greater than 10^{-9} s. If the time delay is greater than 10^{-7} s, the phenomenon is called *phosphorescence* [62].

Photoluminescence is a simple, non-destructive, and contactless analytical technique widely used for investigation of semiconductors. All semiconductors have a

so called energy band-gap (there are no electron states) which separates the valance and conduction band in the energy diagram (Figure 3.3 a)). By illuminating the sample with light (laser) of energy $E_{ex} = hf_{ex} = \frac{hc}{\lambda_{ex}}$ greater than E_g electrons can be excited from their ground state in valance band to excited state in conduction band. Excited electrons can undergo non-radiative relaxation to lower states in the conduction band, and eventually the electron falls back down to the valence band, while emitting a photon. This resulting luminescence is recorded as a plot of emitted photons versus wavelength [63]. This process is schematically described in Figure 3.3 a) and is called intrinsic photoluminescence. Real semiconductor crystals are not ideal and have defects in the crystal structure. These defects (vacancies, dislocations, poor crystal ordering, ...) bring additional electron states into the band gap, and to the measured spectra. Doping the crystal also result in additional electron states. Photoluminescence from this states is called extrinsic [61].

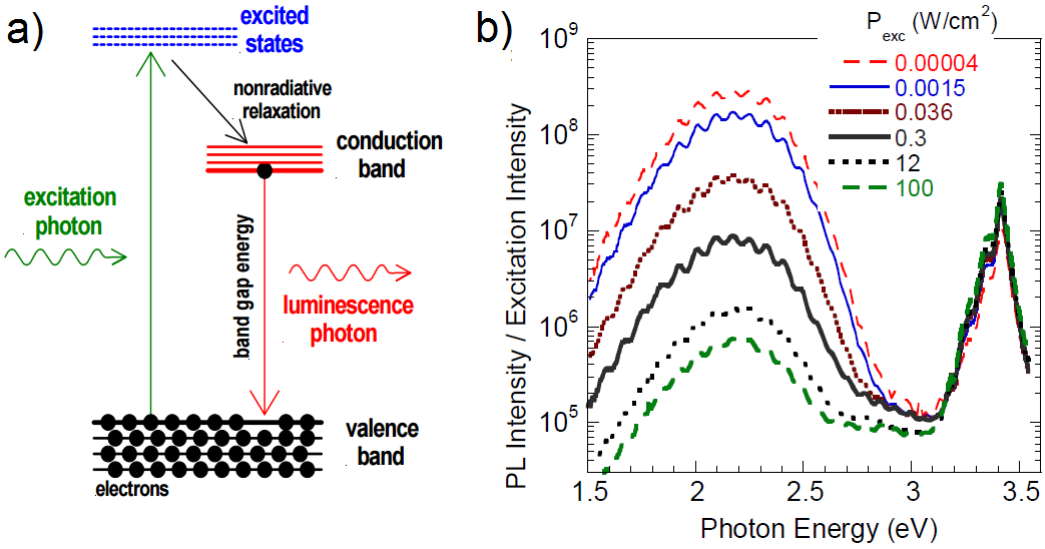

Figure 3.3: a) Schematics of the photoluminescence process. Adapted from ref. [63]. b) Photoluminescence spectra of GaN layers grown on *c*-plane sapphire substrate by MBE. Adapted from ref. [65].

3.2.1 Photoluminescence of GaN

Because GaN has a great potential in optoelectronic applications, photoluminescence is often used to investigate optical properties of prepared GaN. A typical room temperature PL spectrum of GaN is shown in Figure 3.3 b). Two bands are easily distinguished: The first peak with maximum at 3.40 - 3.42 eV (364.7 - 362.5 nm) is the near-bandedge (NBE) emmision peak attributed to annihilation of the free excitons (direct band-to-band recombination between holes in the valance

band and electrons in the conduction band) [64] The second peak positioned at 2.2 eV is the so-called yellow luminescent (YL) peak. The YL peak is typical for MBE and MOCVD preparation methods and is caused by transitions from the conduction band to a deep acceptor, most probably involving a gallium vacancy [65], and typically has a linewidth (FWHM[1]) of about 400 meV [66]. In the PL spectra of GaN other peaks can appear. Green luminescence (GL) peak at 2.4 eV appear due to a combination of gallium vacancy clusters and oxygen (or carbon) impurities. The presence of the blue luminescent peak (BL) at energy 2.75 eV correspond to gallium and nitrogen vacancies and deep level impurities. The correlation between YL and BL and intentional carbon doping was noted by several authors [64].

From the PL spectra the quality of the obtained GaN can be deduced. The main criteria is usually the intensity ration of the NBE and YL peaks. A smaller YL peak reveals higher GaN quality. However, Santana *et al.* have shown, that the ratio depends on the excitation intensity, and it changes rapidly (Figure 3.3 b)). Another criteria is the FWHM of the NBE peak. The smaller the FWHM, the higher the GaN quality. Hong *et al.* [67] have studied the NBE peak dependence on the temperature and on the excitation intensity. They conclude that with increasing the temperature, the FWHM of NBE peak increases and that the excitation intensity does not influence the FWHM.

Determining the GaN quality at room temperature can lead to a wrong conclusion, and therefore, for precise measurements, a low temperature is needed. Nevertheless, many researchers use room temperature PL spectra as a brief insight into the sample quality.

3.3 Enhanced photoluminescence and light-emitting diodes

Among many approaches for the improvement of light-emitting diodes, surface plasmons have been extensively studied to enhance the luminescence efficiency. Surface plasmons (SPs) are collective oscillations of free electrons in a metal that can exist at the interface between metal and dielectric. Confined surface plasmon into a nanoparticle (metal nanoparticle surrounded by dielectric medium) is called localized surface plasmon (LSP). LSP can be excited directly by illuminating the metal nanoparticle with light of resonant frequency. The resonant frequency of LSP depends on the material, size, and shape of the metal nanoparticle, and can be easily tuned. Excited LSP enhance the local electromagnetic field by orders of magnitude. However, this

[1]Full With at Half Maximum

enhancement is strongly dependent on the distance from the metal nanoparticle [68].

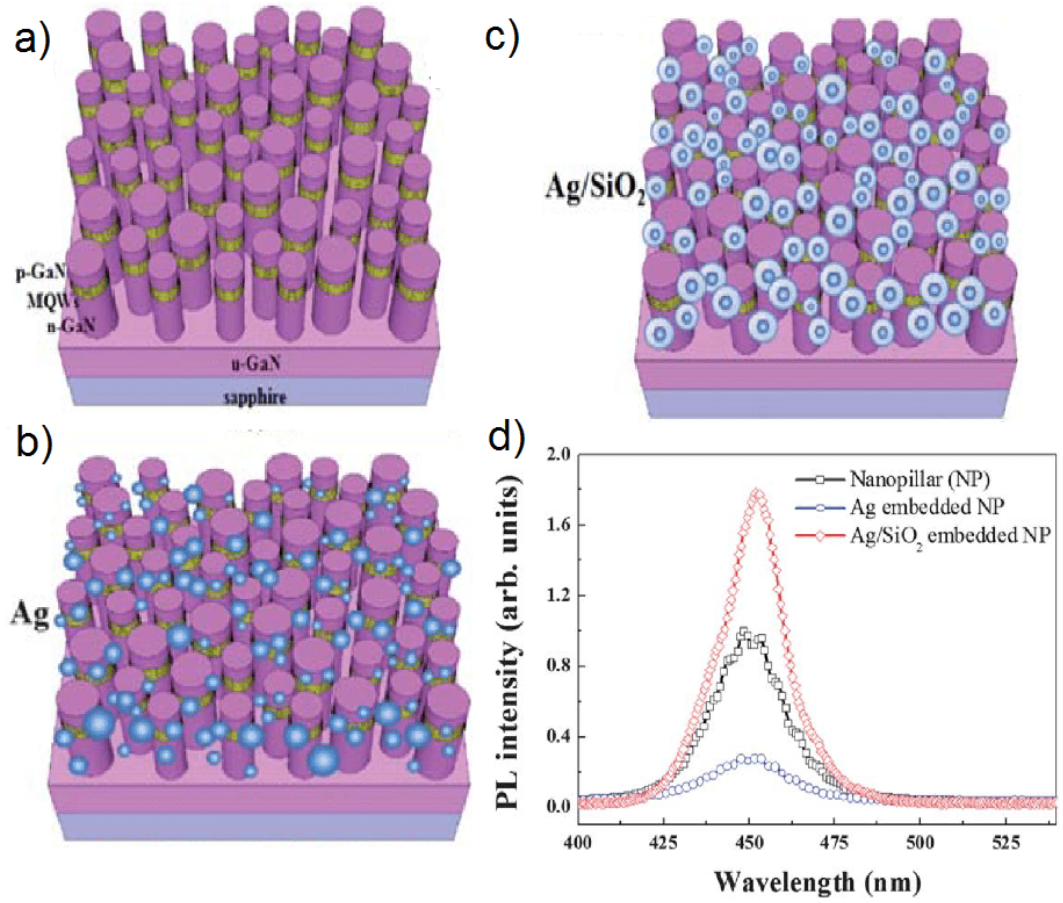

Figure 3.4: a) Schematics of the InGaN/GaN nanopillar LED, b) Ag NP embedded nanopillar, c) and Ag/SiO_2 embedded nanopillar. d) Room temperature photoluminescence spectra of nanopillar LED, Ag embedded nanopillar, and Ag/SiO_2 embedded nanopillar. Adapted from ref. [2].

Recently, LSP phenomena have been used to enhance luminescence efficiency of LEDs by the energy coupling of LSPs with the active quantum well region of the LEDs. Jang *et al.* [2] prepared InGaN/GaN nanopillar LEDs (Figure 3.4 a)) with silver nanoparticles embedded near the active zone (Figure 3.4 b)). In such architecture the NPs are placed very close to the active layer of the LEDs. When the resonant frequency of the LSPs matches the emission energy of the LED, excitons in the active layer of LEDs can transfer their energy directly to the LSP, and thus enhance the luminescence efficiency. However, the PL measurement revealed a decrease in the PL intensity of the Ag embedded sample, shown in Figure 3.4 d). The quenching of PL efficiency in a close-set Ag NPs sample is related to a parasitic

non-radiative energy transfer between Ag NPs. Jang *et al.* eliminated this non-radiative energy dissipation by using Ag NPs with SiO_2 shell (Figure 3.4 c)) instead of mere Ag NPs. The SiO_2 shell separates the Ag NPs and thus prevent the energy dissipation processes. As a result, the PL intensity of a nanopillar LED embedded with Ag/SiO_2 NPs has been increased by 59 %. Similar results have been observed by Cho *et al.* [69] increasing the optical output power of a GaN LED embedded with Ag NP and SiO_2 shell nano-disks by 72 %.

The principle of the enhancement was discussed in more detail by Giannini *et al.* [70]. Radiative properties of a given emitter depend on its environment. In general, the emission intensity of an emitter is given by the product of two different factors: the emitter quantum yield[2] and the electromagnetic energy that an emitter is able to adsorb during excitation, which is proportional to the electric field at the emitter position. Presence of metallic nanoparticles near the emitter can contribute to enhancement of both factors. The LSP resonance increases the local electric field by orders of magnitude (at excitation frequency) and the quantum yield enhancement is related to the possibility to excite LSPs with the emitted photons (at emission frequency). Therefore the highest enhancement can be achieved by cleverly engineered metallic nanoparticles that have two LSP resonances, one that matches with the maximum in the adsorption spectrum of the emitter and another coinciding with the emission frequency. The conclusion from calculations is that the highest enhancement of luminescence occur for emitters with low intrinsic quantum efficiency [71].

3.4 Surface-enhanced Raman spectroscopy (SERS)

Raman spectroscopy is a powerful, non-destructive, and widely used technique that provide molecular fingerprint information. An incident light is inelastically scattered, due to interaction with molecular vibrations (phonons), resulting in an energy shift of the incident photons. The energy shift (Raman signal) provides information about the vibrational modes in the system. The major drawback is its very low cross-sectional scattering and low incident photon flux and thus small detection signal [72].

Surface-enhanced Raman spectroscopy (SERS) has emerged to overcome weaknesses of classical Raman spectroscopy. In SERS, Raman signal can be enhanced by factor 10^{14} using metal nanostructures. Even though SERS effect was discovered over 40 years ago, the mechanism of enhancement is still under debate. At least two mechanisms contribute to the enhancement. Electromagnetic mechanism shows an

[2]Characterize the ability of emitter to radiate once excited.

intense enhancement of the local electromagnetic field in the vicinity of the metal nanoparticle when the energy of the electromagnetic field of the incident light coincides with that of localized surface plasmons (LSP) [73]. Chemical mechanism is based on exchange/transfer of charges between the metal nanoparticle and investigated molecule. The chemical enhancement is small compared to enhancement by LSP and only a small fraction of molecules experience chemical enhancement [74].

SERS has attracted a large interest due to its very high sensitivity and chemical specificity. Although the basic principles of SERS are well established, the development of robust and highly SERS-active substrates is still an active area of research. Among other materials, GaN has been intensively studied as a potential candidate. Wang *et al.* [75] studied SERS effect of Ag nanostructures prepared on epitaxially grown GaN films. Milekhin *et al.* showed, that GaN nanocolums [76] and nanocrystals [77] which have Ag clusters on the surface enhance the Raman signal. Morphology dependent SERS of the substrate supporting the metal NPs was also studied. Sharvani *et al.* [72] prepared a GaN nanowall network which possess a large surface and high conductivity. The result of this study revealed a large enhancement factor and low limit of detection for sharp nanowall morphology embedded with Ag NPs compared to blunt nanowall surface.

A room temperature Raman spectrum of wurtzite GaN film prepared on sapphire(0001) substrate is shown in Figure 3.5. The most intense E_2 peak is positioned at 567 cm^{-1} and the A_1(LO) peak at 734 cm^{-1}. The width of the E_2 peak is associated with the crystalline quality. The position of the E_2 shifts linearly with stress. Shifts to higher frequencies indicate compressive stress, whereas shifts to lower frequencies correspond to tensile stress in the GaN film. Information on the free carrier concentration can be deduced from the A_1(LO) peak. With higher free carrier concentration the peak shifts to higher frequencies and broadens [78].

Up to now, all the samples for SERS effect study of metal NPs on GaN substrates were prepared in two steps. Firstly, the GaN structures (film, nanorods, nanocrystals, ...) were prepared and secondly, the metal NPs were embedded. The preparation of GaN nanocrystals with metal core in our work is directly opposite, firstly metal NPs are deposited on the substrate and afterwards a GaN crystal is formed over the metal NP. We believe that such a prepared structure will exhibit strong SERS effect.

Among many potential applications of SERS, UV SERS and chemical sensing in a caustic environment are the main interest of our work. We believe that GaN grown over a metal nanoparticle will prevent the metal nanoparticle from degradation, and thus enable manufacturing high durability sensors for caustic environments. UV SERS is highly desirable because it would enable resonant detection of many bi-

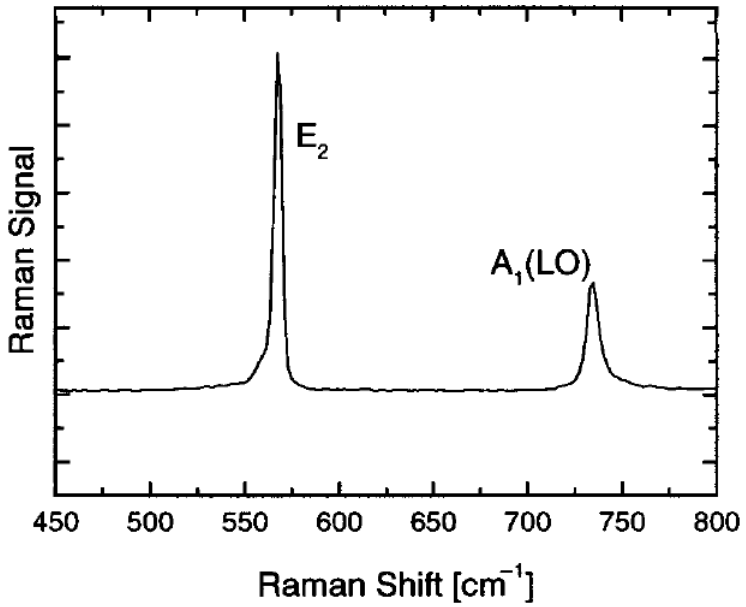

Figure 3.5: Room temperature Raman spectrum of wurtzite GaN film prepared on sapphire(0001) substrate. Adapted from ref. [78].

ological molecules, including protein residues and DNA bases. For this reason we believe that GaN nanocrystals with Al core can contribute to UV SERS because LSP resonance of Al spheres can be tuned to the UV region [79].

4 PREPARATION OF GAN NANOCRYSTALS WITH THE METAL CORE

The growth of GaN at the Institute of Physical Engineering in Brno has been studied for many years. The main interest of the research is the preparation of high quality GaN crystals, selective GaN growth, growth on different substrates,... With the previous knowledge of the IBA-MBE GaN growth at low temperatures and the metal NP deposition we want to prepare GaN crystals with the metal core. Within the aims of this work is also characterization of prepared structures.

The preparation of GaN crystals with the metal core consists of three steps:

1. Deposition of metal nanoparticles,
2. Ga deposition,
3. Post-nitridation process.

4.1 Deposition of metal NPs

The theory behind the deposition process was discussed in section 3.1. In our experiments we have used Ag NPs with 40 nm diameter made by BBInternational company and delivered in colloidal solution. As a substrate the Si(111) with native SiO_2 was used. The pH of the colloidal solution is $\sim$ 5.5, whereas the isoelectric point of the Si(111)/SiO_2 is at pH $\sim$ 3.5. Therefore an acid has to be added into the solution. We have tried to use hydrofluoric acid (HF) and hydrochloric acid (HCl). The best results have been achieved with 2.5 mM HCl[1] modified solution. In Figure 4.1 a) and b) are shown SEM images of samples immersed into a 2.5 mM HCl modified solution for t = 20 min and t = 60 min, respectively. The longer the sample is immersed, the higher the concentration of NPs is expected [55].

Our results confirm that the NP concentration is proportional to immersion time, but after t $\sim$ 30 min, NPs start to agglomerate (Figure 4.1 b)). For our purpose, the ideal distance between NPs is $\sim$ 1 μm, which correspond to immersion time t = 20 min (Figure 4.1 a). Not all NPs are deposited separately, $\sim$ 20% of deposited NPs form dimers, and $\sim$ 4% form trimers. Even though dimers and trimers are undesirable, their presence cannot be easily eliminated. Ag NPs deposition in all further experiments was done by immersing Si substrate in 2.5 mM HCl modified solution fot t = 20 min.

Ga deposition was done by MBE in UHV conditions. Prior Ga deposition, sample with Ag NPs has to be annealed to remove stabilizing agents (citrates) and other

[1] to 1 ml of colloidal solution is added 1 μl of 5% HCl

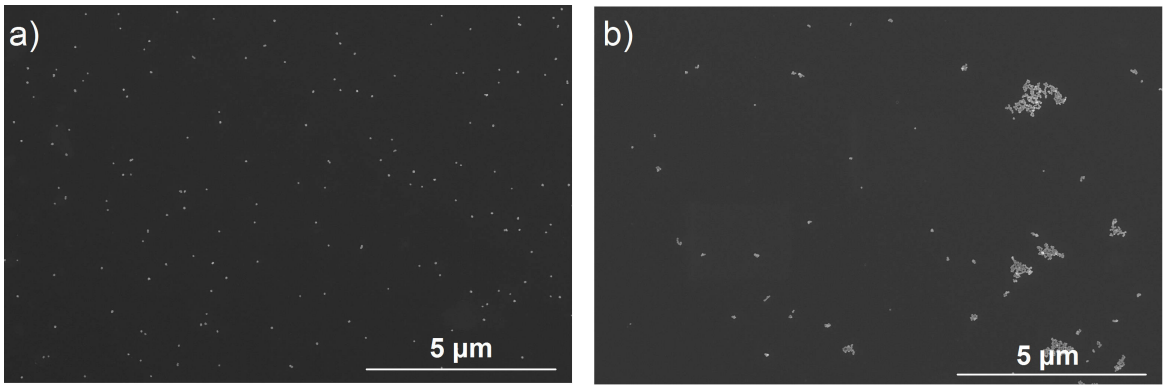

Figure 4.1: SEM images of deposited 40 nm Ag NPs on the Si(111) substrate with native SiO_2. The samples were immersed into a 2.5 mM HCl modified colloidal solution for a) $t = 20$ min, b) $t = 60$ min. Agglomeration of Ag NPs is not desirable for further experiments. Images taken in CEITEC on FEI Verios 460L.

hydrocarbons from the surface. To achieve uniform annealing over the whole sample, direct current flow through Pyrolytic Boron Nitride (PBN) heating element was used. PBN is often used because it is non-reactive to most other compounds, has high thermal conductivity, high dielectric strength, and high insulation resistance.

Usually, we have annealed our samples to temperatures $T = 250°C$ - $350°C$ for $t = 120$ min. It was found that after annealing the shape of deposited Ag NPs change from spherical (Figure 4.2 a)) to more hemispherical shape (Figure 4.2 b)). Consequently, the diameter increases from ~ 40 nm to ~ 60 nm. During annealing the stabilizing citrate molecules are removed from the Ag NPs surfaces and the Ag NPs start wetting the substrate. Therefore their shape changes to hemispherical. This change will certainly affect the properties of LSP excited on the Ag NP.

4.2 Ga deposition

Deposition experiments were performed in a laboratory of the Institute of Physical Engineering in Brno, in the complex UHV apparatus schematically described in Figure 4.3. The apparatus consists of an analysis chamber, where X-ray photoelectron spectroscopy can be measured, and of a deposition chamber, where Ga effusion cell and N_2^+ ion source were mounted to enable GaN preparation. The principle of Ga effusion cell and the N_2^+ ion source were described in section 2.2.3.

For Ga deposition the substrate temperature T_s and the flux of Ga atoms J are the key parameters determining the processes of the impinging Ga atoms on the

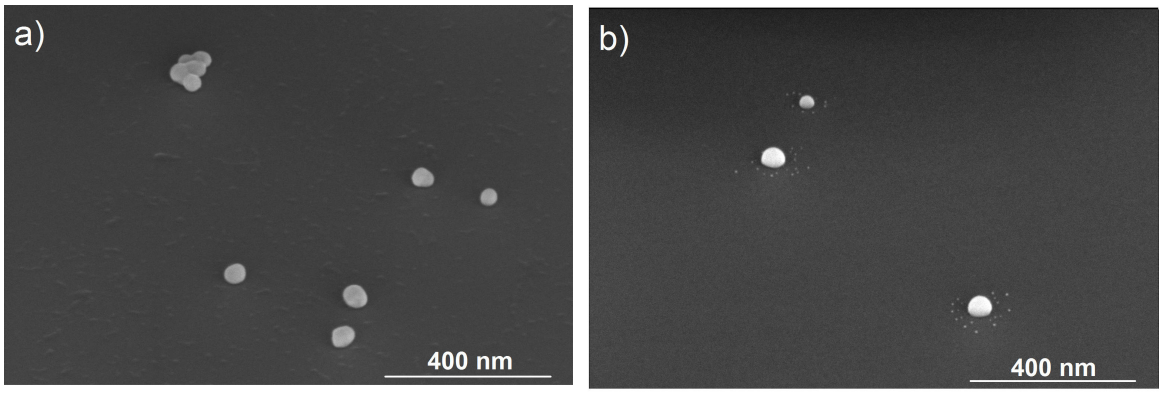

Figure 4.2: a) SEM image of a 55° tilted sample with Ag NPs. NPs have approximately spherical shape with diameter $\sim$ 40 nm. b) After annealing to T = 300°C for t = 120 min the stabilizing citrate molecules are removed from the NP surface and the NP start wetting the substrate. Therefore they change their shape to hemispheres with diameter $\sim$ 60 nm. Images taken in CEITEC on FEI Verios 460L.

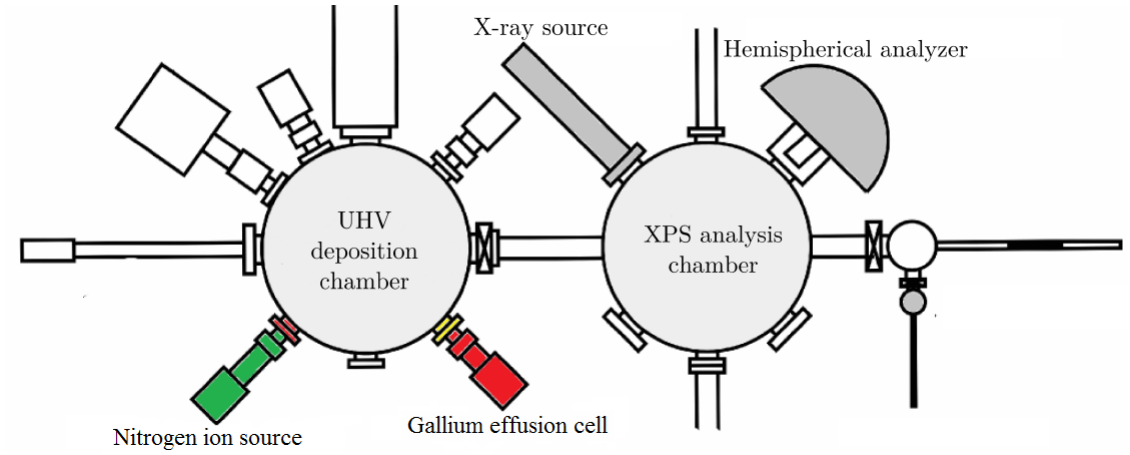

Figure 4.3: A schematic of a complex UHV apparatus at the Institute of Physical Engineering in Brno used for GaN preparation. Adapted from ref. [34].

surface. If the T_s is sufficiently high and J small, diffusion of the Ga adatoms toward the Ag NPs can be expected. Five Ga depositions on the previously deposited Ag NPs on the Si(111) substrate with native SiO_2 were done at different T_s (T_s = 250, 270, 290, 330, 350°C) and with fixed J. In our experiments we did not measure the exact value of J. We measured a current I_J of ionized Ga atoms, which is proportional to the flux J of neutral Ga atoms, as was discussed in section 2.2.3. For the first depositions the parameters of the Ga effusion cell were set to values: filament current I_F = 29.8 mA, accelerating voltage on the crucible U = 800 V, and the I_J = 77 nA. The I_J = 77 nA corresponds to $1{\times}10^{16}$ atom·cm^{-2}·h^{-1}, as we know from previous calibration. As a result of the five Ga depositions at different T_s, T_s = 290°C was found to be suitable for Ga deposition on Ag NPs. In the Figure 4.4 a) a SEM image after Ga deposition at T_s = 290°C is shown.

In scanning electron microscopy two types of electrons can be detected to create an image. Secondary electrons (SE) with energy $E < 50$ eV provide information about morphology and surface topography, whereas back-scattered electrons (BSE) with $E \geq 50$ eV are more sensitive to a material of the sample. In our SEM measurements we were mainly interested in the material composition, therefore the BSE electrons were detected.

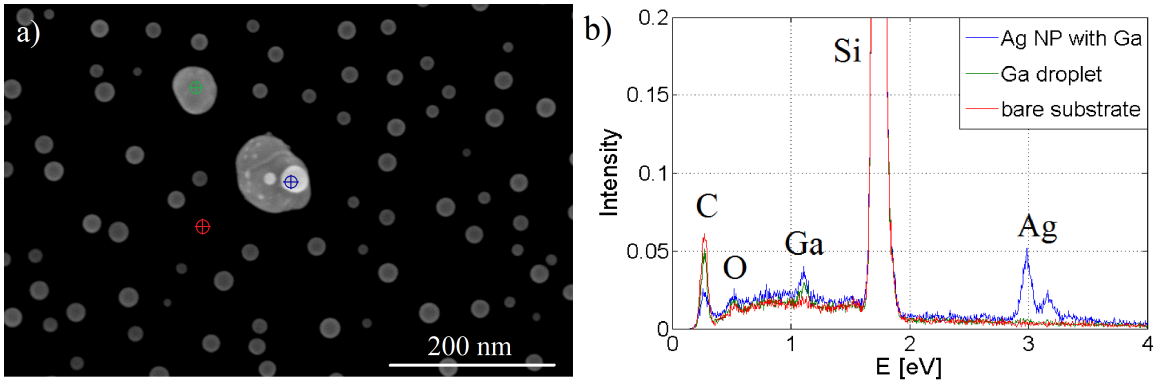

Figure 4.4: a) SEM image of Ga droplets grown on 40 nm Ag NPs previously being deposited on the Si(111) substrate for t = 120 min at substrate temperature T_s = 290°C. To sense the material contrast, back scattered electrons (BSE) were detected. The different contrasts in the image were identified using EDX analysis. The brightest features were assigned to be Ag, and the less bright Ga. b) EDX spectra color-matched with the points in image a). Image and spectra taken in CEITEC on FEI Verios 460L.

To assign the different contrasts in the SEM image in Figure 4.4 a) to a certain

chemical element, an energy-dispersive X-ray spectroscopy (EDX) was used. Spectra taken at different points (color-matched sun crosses in SEM image 4.4 a)) are shown in Figure 4.4 b). The brightest features were found to be silver and the less bright Ga droplets on the surface.

During deposition of Ga, the substrate temperature $T_s = 290°C$ is suitable because the Ag NPs are inside relatively large Ga droplets ($\sim$ 100 nm in diameter). In an ideal case, we would like to have Ga only around Ag NPs. To eliminate the presence of small Ga droplets (not containing Ag NPs), T_s has to be elevated to enhance the diffusion length of Ga adatoms (sufficiently to reach the nearest Ag NP). Depositions at $T_s = 330$ and $350°C$ (images not shown here) revealed that these temperatures are already too high, because almost no Ga was present on the surface. This is because the desorption probability increases with increasing T_s, in other words the sticking coefficient of Ga atoms on the SiO_2 surface is lowered, resulting in desorption of most of the impinging Ga atoms at higher T_s. Lowering the T_s to $T_s = 250°C$ decreases the diffusion length of Ga adatoms and therefore Ag NPs are surrounded by smaller Ga droplets ($\sim$ 65 nm in diameter) and more small Ga droplets are present on the surface (images also not shown here).

The SEM image in Figure 4.4 a) shows one more feature. The central large Ga droplet contains one bigger ($\sim$ 30 nm) and many small Ag NPs. This was surprising because Ag NPs were expected to be stable. To understand what has happened during the Ga deposition a Ag-Ga phase diagram is needed, shown in Figure 4.5. In a Ag-Ga phase diagram it is seen that for $T_s = 290°C$ almost 15% of Ag dissolves in Ga. After deposition when the sample is cooling down, the dissolved Ag segregate to the Ga droplet surface. To prove this statement our sample was investigated by Auger electron spectroscopy (AES) on the nanoScanning Auger microscope in CEITEC.

Scanning Auger Microscopy (SAM) or Auger Electron Spectroscopy (AES) is an analytical technique used in surface physics to determine the elemental composition. In this technique a focused primary electron beam scans over the surface of interest. As a result of the interaction between the primary electron beam and the sample, Auger electrons are emitted from near the surface region (0.5-5 nm). By detecting these Auger electrons a SAM image is formed. The Auger electrons escape from the surface with certain kinetic energy characteristics of the parent atom. By analyzing the kinetic energy of the Auger electrons a spectrum containing the information on the elemental composition of the sample is formed. SAM/AES take place in UHV conditions [81].

Our sample (Ga droplets with Ag NPs) was imaged by SAM, Figure 4.6 a). The SAM image is similar to the SEM image in Figure 4.4 a). AES spectra taken at the region defined by cross in SAM image 4.6 a) are shown in Figure 4.6 b). If the

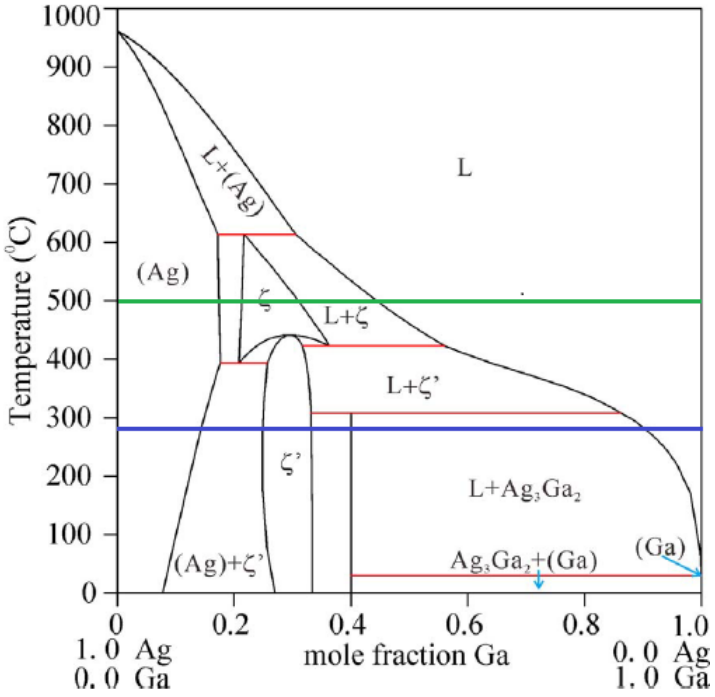

Figure 4.5: Ag-Ga phase diagram. Adapted from ref. [80]

Ag NPs were stable during Ga deposition, no Ag peak should be detected in this region. In AES spectra a clear Ag MNN peak positioned at energy $E = 358$ eV is seen. Further evaluations of spectra taken at different points (not shown here) are in accordance with EDX measurements: The brightest features correspond to Ag and the darker features to Ga. Because of the surface sensitivity[2] of SAM/AES segregation of dissolved Ag in Ga to surface when cooling down can be confirmed. One more piece of information from the AES spectra supports our hypothesis. The presence of a small peak positioned at energy $E = 354.2$ eV (highlighted in green) corresponds to Ag_2SO_4 compound. We believe that this compound is formed when segregated Ag on top of Ga droplets react with air[3].

SEM/EDX and SAM/AES measurements show that during Ga deposition Ag NPs are not stable. Phase diagram and AES suggest that Ag dissolve in Ga (at temperate T = 290°C) and when cooled down Ag segregate on the Ga droplet surface. This process is undesirable because changes in the shape and size of Ag NPs modify their plasmonic properties and also the presence of small Ag NPs in the Ga droplet will cause defects in following GaN formation. Dissolution of Ag in Ga has to be eliminated, therefore several approaches were proposed:

[2]The information depth is limited by the mean free path of Auger electrons traveling through a material, which is typically in 0.5-5 nm [81].

[3]Air contains a small fraction of sulfur dioxide SO_2.

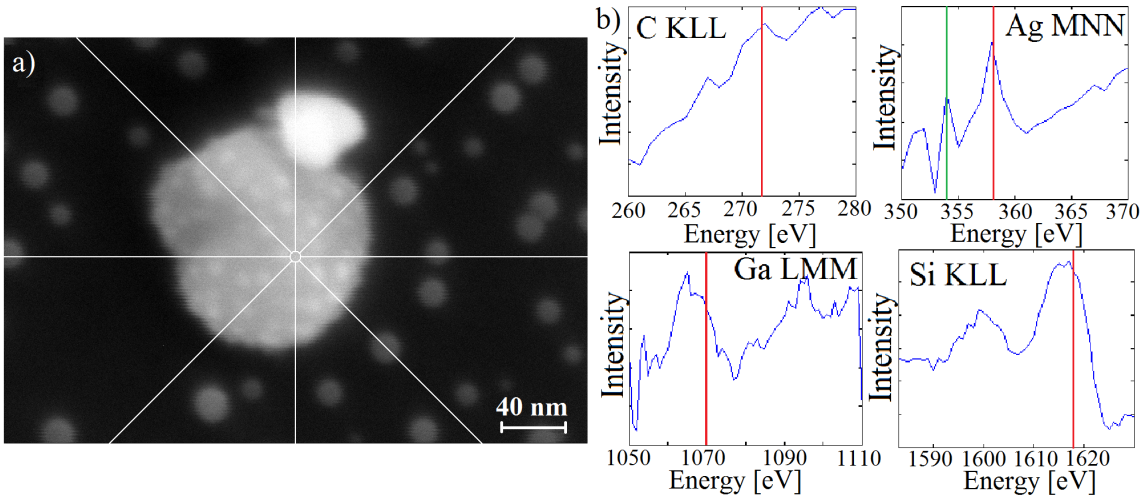

Figure 4.6: a) Scanning Auger Microscopy (SAM) image after Ga deposition on the Si(111) substrate with Ag NPs. b) Auger electron spectra taken at the region defined by the cross in the SAM image. A clear Ag MNN peak positioned at energy $E = 358$ eV in the AES spectra confirm dissolution and following segregation of Ag NPs.

- Ga deposition at higher substrate temperature.
- Ga deposition on Ag NPs overlaid by graphene.
- Passivation of Ag NPs in the air.
- Atomic layer deposition of 2 nm SiO_2 on the Ag NPs previously deposited on substrate.

4.2.1 Ga deposition at higher T_s

In the first Ga deposition series T_s was varied from $T_s = 250°C$ to $T_s = 350°C$. For these temperatures some Ag dissolve in Ga. The idea to eliminate the dissolution by depositing Ga at higher T_s comes from the phase diagram. For temperature $T_s = 500°C$ (green line in Figure 4.5) ζ phase is present. We believe that the ζ phase might be stable and therefore prevent the Ag dissolution.

A support of our ideal was found in one of the previous work at the Institute of Physical Engineering in Brno [60]. In this work 20 nm and 40 nm Ag NPs were deposited on the Ge(111) in the same way as we have done. Afterwards Ga was deposited at substrate temperature $T_s = 500°C$. According to their results, no Ag dissolution in Ga was observed.

After Ga deposition at $T_s = 500°C$ and $t = 60$ min a SEM image in Figure 4.7 a) was taken. In the image it is seen that no Ga is present on the surface. Even

though the sticking coefficient of Ga on SiO_2 is almost zero at $T = 500°C$ some of the Ga adatoms that reach Ag NP can nucleate there. To increase the sticking coefficient, SiO_2 was etched away by immersing new sample with Ag NPs into 5% HF for $t = 1$ min. A SEM image after Ga deposition at $T_s = 500°C$ and $t = 60$ min is shown in Figure 4.7 b). Because the situation is similar to image a) we conclude that another approach to eliminate Ag dissolution has to be found.

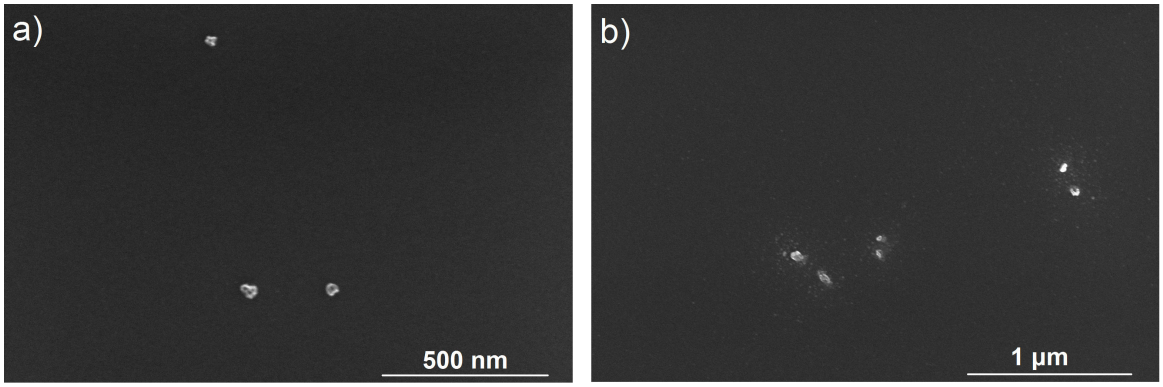

Figure 4.7: a) SEM image after Ga deposition at $T_s = 500°C$ and $t = 60$ min. b) SEM image of a sample where SiO_2 was etched away and then Ga deposition at the same parameters was done. Due to low sticking coefficient no Ga is present in both images. Images taken in CEITEC on FEI Verios 460L.

4.2.2 Ga deposition on Ag NPs overlaid by graphene

On the Si(111) substrate 40 nm Ag NPs were deposited in the same way as in the previous experiments. After Ag NPs deposition the sample was annealed in UHV conditions at $T = 350°C$ for t = 45 min to remove the stabilizing agent (citrate) from the Ag NP surface. During annealing Ag NPs change their shape to hemispherical, as previously showed in Figure 4.2 b). The annealed sample was carried out of the UHV conditions and overlaid by a CVD graphene flake[4]. Before Ga deposition, the sample was cleaned by annealing in UHV at $T = 400°C$ for t = 120 min. The Ga deposition was carried out at $T_s = 290°C$, t = 60 min, and flux $I_J = 77$ nA.

A SEM image of the sample after deposition is shown in Figure 4.8. At a first look it is difficult to assign different contrasts to different elements. Because of a certain knowledge of Ga deposition on graphene in our group [34, 83] we can speculate that the brightest features (circled in red) correspond to Ag NPs overlaid by graphene

[4]CVD (Chemica Vapor Deposition) graphene was prepared by Ing. Pavel Procházka [82].

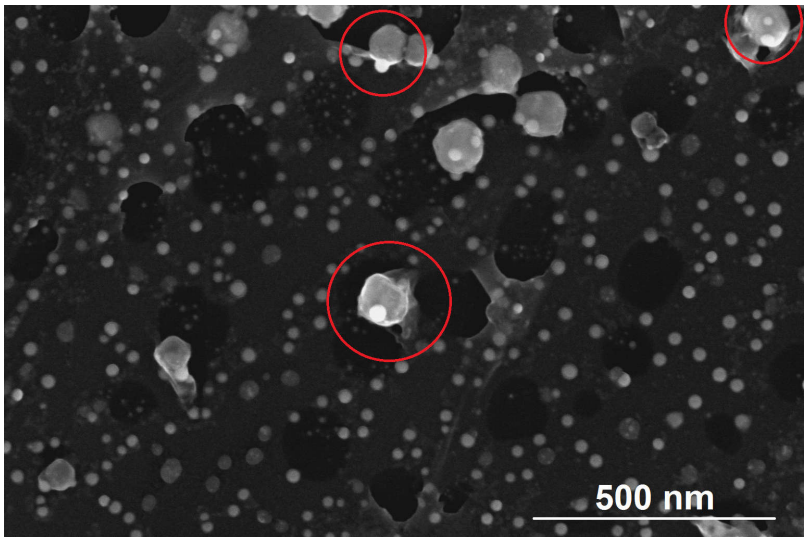

Figure 4.8: A secondary electron SEM image of Ga deposited on Ag NPs overlaid by CVD graphene. The features circled in red are believed to be large Ga droplets on top of Ag NPs overlaid by graphene. Images taken in CEITEC on FEI Verios 460L.

and surrounded by Ga. For more precise understanding of structures formed on the surface different analytical techniques have to be used.

Concerning dissolution of Ag in Ga, from the SEM image a clear conclusion can not be reached. For complexity and time reasons, further studies of deposited Ga on Ag NPs overlaid by graphene were not developed.

4.2.3 Passivation of Ag NPs in the air

The idea of passivating Ag NPs in the air came from a fact that Ag immediately oxidize when exposed to the air. A created silver oxide shell on top of the Ag NP might protect Ag dissolution during Ga deposition. In the literature [84] was found that naturally occurring oxide thickness of Ag_2O on silver exposed to the natural oxygen environment is in the range 10 to 20 Å. A room temperature dependence of native oxide thickness of various metals on exposure time to natural oxygen environment is shown in Figure 4.9 a). From this plot it is seen that after 24 hours the thickness of Ag_2O, $t_{Ag_2O} = 1.2$ nm. During Ga deposition substrate temperature $T_S = 290°C$ is needed, and therefore Ag_2O shell has to be thermally stable up to this temperature. According to [85], Ag_2O is stable until 350°C.

Ag NPs were deposited on the Si(111) substrate in a regular manner and then annealed in UHV to $T = 290°C$ for $t = 120$ min to remove citrate molecules from the Ag NPs. A sample was carried out of a vacuum and left for t = 19 hours in

the air. In the next step, the sample was again annealed in UHV to $T = 250°C$ for $t = 120$ min and then Ga was deposited for $t = 60$ min, with $T_S = 290°C$, and flux $I_J = 77$ nA.

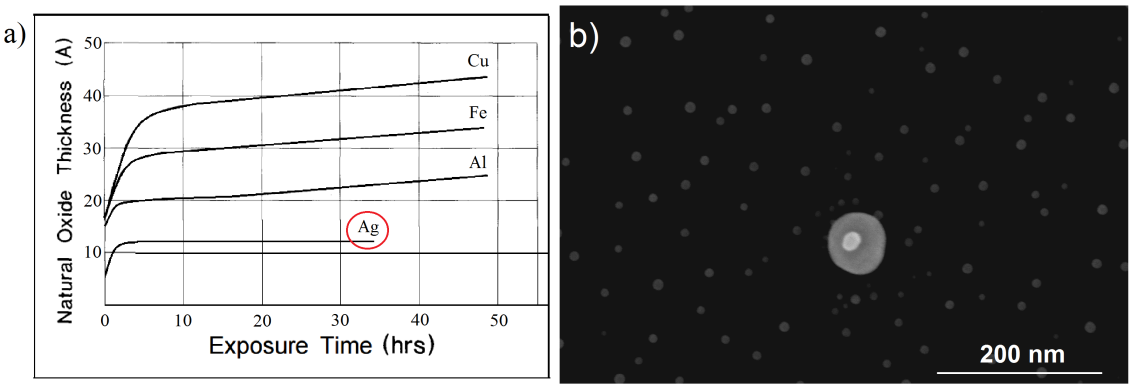

Figure 4.9: a) Thickness of a native oxide formed on various metals at room temperature. Adapted from ref. [84]. b) BSE SEM image of the sample after Ga deposition. Before Ga deposition Ag NPs were annealed and left outside vacuum to oxidize for t = 19 hours. As seen from the image, the created oxide shell prevents Ag from dissolving in Ga during deposition. Image taken in CEITEC on FEI Verios 460L.

A BSE SEM image shown in Figure 4.9 b) was made after Ga deposition. From this image it is clearly seen that there is only one Ag NPs in the large Ga droplet (as compared with image in Figure 4.4 a)). Apparently the thickness $t = 1.2$ nm of Ag_2O is sufficient to prevent dissolution of Ag into Ga during Ga deposition. This ascertainment solves our problem with Ag dissolution and enables us to prepare high quality GaN crystals with the Ag core.

4.3 Preparation of GaN nanocrystals with the Ag core

The third step in preparation of GaN crystals with the Ag core is the post-nitridation, where Ga droplets are transformed into GaN crystals. In this process hyperthermal N_2^+ are needed. The source of hyperthermal N_2^+ as well as the principle of post-nitridation process was discussed in section 2.2.3.

Samples used in previous experiment (Ga deposition) cannot be used, because once taken out of UHV, an oxide forms on the Ga droplets and block the GaN transformation. For this reason new samples had to be prepared. 40 nm Ag NPs

were deposited on the Si(111) substrates by immersing the Si(111) into 2.5 mM HCl modified colloidal solution for $t = 20$ min. In the next step the samples were annealed in UHV at temperature $T = 290°C$ for $t = 120$ min. By annealing stabilizing citrate molecules are removed from the Ag NP surface. When taken out of UHV and left $t = 22$ hours in the air, thin silver oxide layer is formed. Samples were then again annealed in UHV at $T = 290°C$ for $t = 120$ min to clean the sample prior Ga deposition. GaN cryxtals with the Ag core were prepared on two samples, denoted Sample 1 and Sample 2.

In the Sample 1, Ga deposition was done at $T_S = 290°C$ for $t = 120$ min with flux $I_J = 77$ nA. After Ga deposition the sample was kept at the same temperature ($T_S = 290°C$) to enable diffusion of Ga adatoms to form larger Ga droplets. In the post-nitridation process a broad beam of N_2^+ ions with energy $E = 50$ eV was irradiating the surface. Post-nitridation was performed for $t = 180$ min and the sample was kept on the temperature $T_S = 200°C$. After the post-nitridation, the substrate temperature was elevated to $T_S = 400°C$ for $t = 20$ min. Ga that was not transformed into GaN during post-nitridation desorb at this temperature and only GaN crystals are left on the surface.

The Sample 2 was treated almost in the same way. The difference was in the Ga deposition time, $t = 60$ min, and the post-nitridation time, $t = 120$ min. The Sample 2 was not annealed at the end.

From X-ray Photoelectron Spectroscopy (XPS) measurements the transformation of Ga into GaN can be checked. For metallic gallium the Ga $2p_{3/2}$ peak is positioned at binding energy $E_B = 1117$ eV. After transformation of Ga to GaN the Ga $2p_{3/2}$ peak shifts to higher binding energy $E_B = 1118.7$ eV. In our measurements the whole XPS spectra were shifted by ~ 4.5 eV to the higher binding energy[5]. XSP spectra of the Ga $2p_{3/2}$ peak measured on the Sample 1 after post-nitridation are shown in Figure 4.10. The blue curve shows the measured date. Fitting the peak in the XPSPeak software shows that there is $\sim 80\%$ of GaN and $\sim 20\%$ of metallic Ga on the surface. Even though the sample was annealed after post-nitridation to remove surplus Ga, some Ga is still present on the surface. This is related to the mechanism of the post-nitridation process. In a certain point the growing GaN crystal can cover the Ga-residues and the impinging nitrogen ion cannot bind to the Ga atom on the structure anymore [34]. In the XPS spectra no Ag peak was detected. Because of the surface sensitivity of XPS it could mean that the Ag NPs are not on the surface but incorporated in the GaN structures. Unfortunately, after measuring XPS spectra of Ag NPs deposited on the Si(111) substrate we have to conclude that the concentration of Ag NPs is too low to be measured by used XPS.

[5]The work function instrumental correction factor was not set properly.

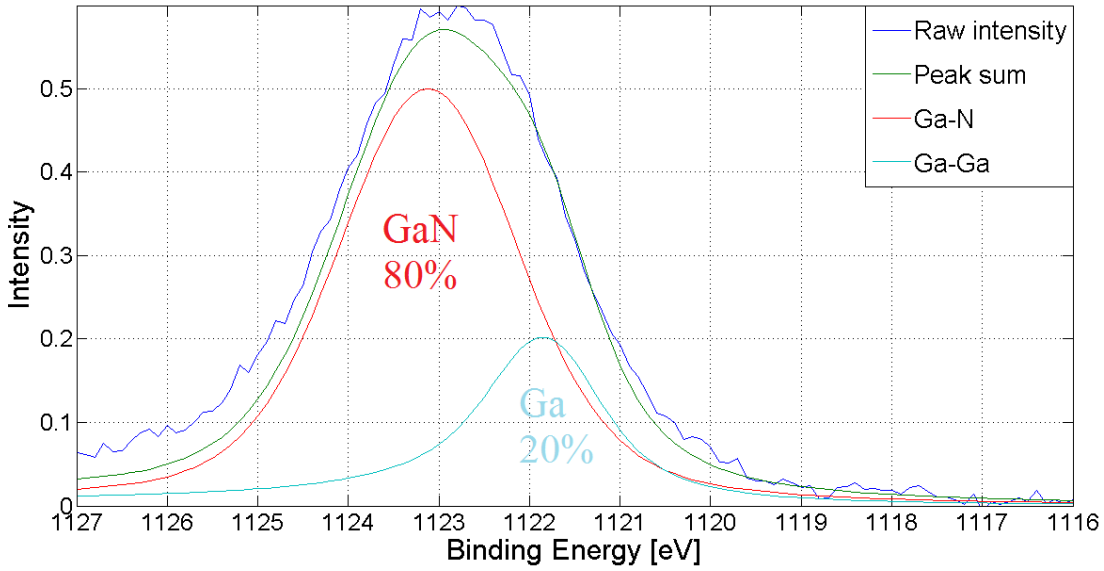

Figure 4.10: XPS Ga $2p_{3/2}$ peak measured after $t = 120$ min Ga deposition, $t = 180$ min post-nitridation, and then $t = 20$ min annealing at $T = 400$°C. Measured data (blue curve) were fitted in the XPSPeak software. The red peak positioned at $E_B = 1123.2$ eV correspond to GaN and the turquoise peak at $E_B = 1121.8$ eV to metallic Ga.

Samples were also investigated in SEM. In Figure 4.11, BSE images of the Sample 1 are shown. This sample was annealed at the end of post-nitridation (to remove spare Ga), therefore only GaN crystals should remain on the surface. In Figure 4.11 a) the sample is not tilted. We believe that the central large feature is a GaN crystal containing an Ag NP. Because of the sensitivity of BSE to material contrast (to atomic number Z) the bright feature (pointed by an arrow) is an Ag NP. The small features surrounding the central GaN crystal are the ever-present small Ga droplets (e.g. Figure 4.9 b)) transformed into GaN. BSE image in Figure 4.11 b) was taken with 55° tilted sample. The large GaN crystal containing Ag NP (bright feature) seems qualitatively the same as in Figure 4.11 a). In both images an inkling of hexagonal crystal shape is seen.

In Figure 4.11 b) or in zoomed image c) is clearly seen that part of the small Ga droplets were transformed into rod/wire structure and the other part into crystals. This is surprising because in the previous work on GaN growth in our group rod/wire features were not observed. The origin and the composition of the rods/wires is not certain. The small crystals are formed in the same manner as the large ones, forming GaN. In Figure 4.11 c) it is seen that on top of each rod/wire a sphere is present. This might be the Ga droplet acting as a catalyst, as described in section 2.3.1.

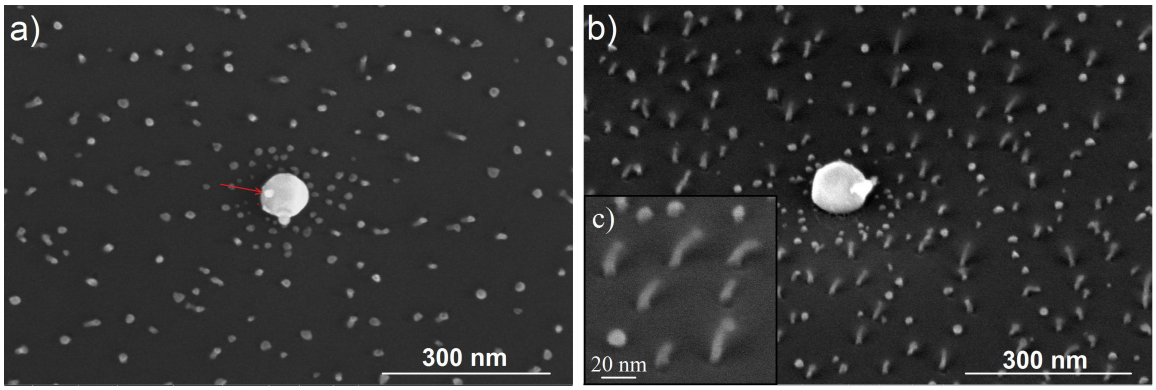

Figure 4.11: BSE SEM images of prepared GaN crystals with the Ag core. a) 0° tilted image of the sample. The brightest feature (pointed by the arrow) is believed to be Ag NP. b) 55° tilted image and c) zoomed image surprisingly reveal formation of rods/wires. The composition and origin of the rods/wired is not clear. Images taken in CEITEC on FEI Verios 460L.

The rods/wires in the image are sharp close to the surface but further they become blurred, as if the rods/wires were not well conductive. This raises uncertainty over the composition of the rods/wires. Further studies of the origin and composition of the formed rods/wires has to be done in the future.

4.4 Photoluminescence of GaN with the Ag core

On our two samples with GaN crystals with the Ag core photoluminecsence spectra were measured. GaN at room temperature has a bandgap of $E_g \sim 3.4$ eV, corresponding to wavelength $\lambda = 365$ nm. For this reason a $\lambda = 325$ nm He-Cd laser was used for excitation. Figure 4.12 shows the measured spectra. The referential spectrum (blue) was taken on the edge of our sample, where only Ag NPs are present on the Si substrate. Unfortunately our GaN crystals (positioned in the center of our sample) are too small to be seen in optical microscope and therefore spectra were blindly measured. Most of the spectra looked like the green spectrum. In average every 10^{th} spectrum was different (red and black spectrum in the Sample 1 and Sample 2, respectively) showing a peak corresponding to GaN NBE peak positioned at $\lambda \sim 365$ nm. The red and black spectra are believed to be taken from a single GaN crystal with the Ag core and the green spectrum is taken from regions between GaN crystals where the small GaN crystals and rods/wires are present. The blue and green spectra are almost identical, therefore we can conclude that the small

GaN crystals and rods/wires do not show any detectable photoluminescence.

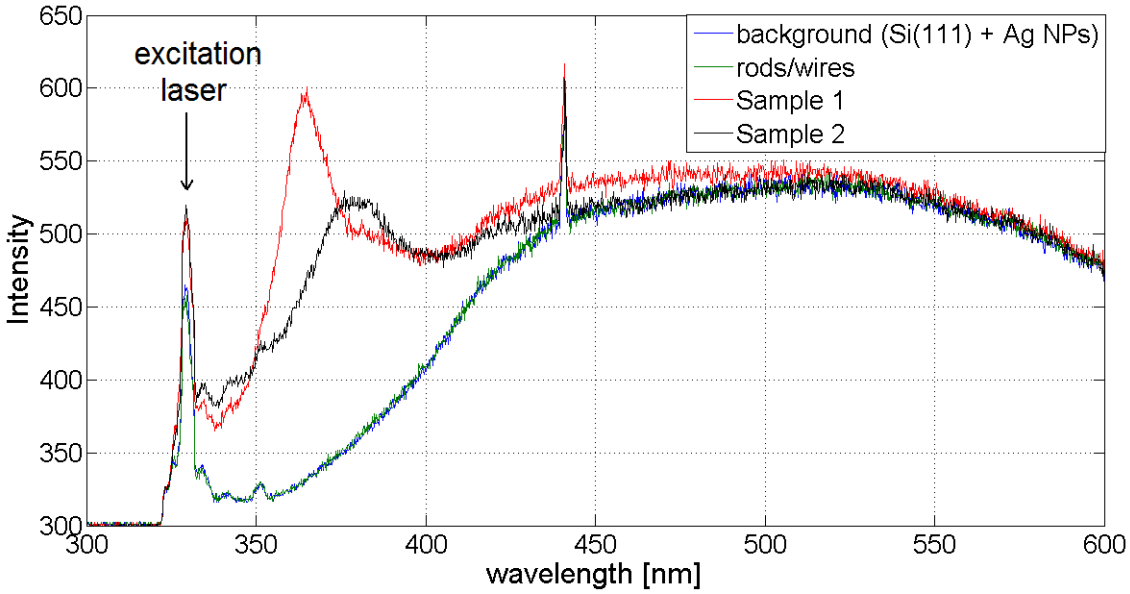

Figure 4.12: Photoluminescence spectra of our samples of GaN crystals with the Ag cores. The blue spectrum is referential (the Si(111) substrate with Ag NPs), the black spectrum corresponds to a region where only small GaN crystals with rods/wires are present. The green and red spectra are taken from a single GaN crystal with the Ag core from Sample 1 and Sample 2, respectively.

The spectra taken from the GaN crystals with the Ag core and the reference spectrum (Si substrate with Ag NPs) were subtracted. The result is seen in Figure 4.13. Interestingly, only one peak positioned at $\lambda = 365$ nm and $\lambda = 376$ nm for Sample 1 and Sample 2, respectively is seen. This NBE peak is characteristic for high quality GaN crystals. The NBE peak of Sample 2, is red-shifted and broader as compared to the NBE peak of Sample 1. The FWHM of the NBE peaks are 22 nm and 36 nm for Sample 1 and Sample 2, respectively. The red-shift and broadening of the NBE peak is probably connected to the presence of residual Ga on the GaN crystals, because the Sample 2 was not annealed after post-nitridation process.

Usually the YL peak positioned at $\lambda = 563$ nm referring to defects in the crystals is seen in the spectra. The reason why the YL peak is not seen in our measurements is either high quality of the prepared GaN crystals with the Ag core, or might be caused by the presence of Ag NPs. To understand the spectra in more detail, further study is needed.

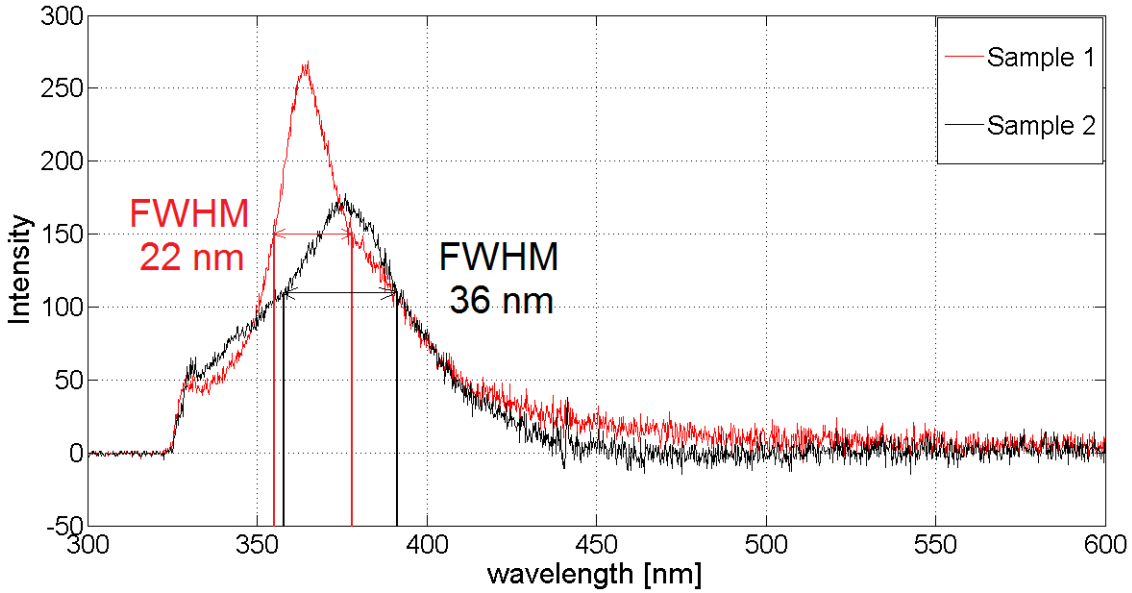

Figure 4.13: Photoluminescence spectra taken from a single GaN crystal with a Ag NP subtracted by the reference spectrum (Si substrate with Ag NPs). Only the NBE peak referring to high quality GaN crystals is present.

4.5 Raman spectroscopy of GaN with the Ag core

We wanted to test to see if our GaN crystals with the Ag core will exhibit the SERS effect or not. A green laser ($\lambda = 532$ nm) was used to irradiate the sample. Measured Raman spectra are shown in Figure 4.14. The blue curve was measured on the Si(111) substrate where only Ag NPs were deposited. The green curve was measured on the Sample 1. There is no detectable difference in the two spectra, therefore we conclude that the SERS effect of the prepared GaN crystals with the Ag core was not proven.

4.6 GaN nanocrystals with the Al core

GaN crystals with the Al core are highly desirable because the LSP resonant frequency of Al nanospheres is positioned in UV region. Within this work, few experiments with Ga and GaN deposition on Al NPs on the Ge(111) substrate were done. The Al NPs were not deposited from the colloidal solution. Al NPs were formed in UHV conditions by depositing a 0.75 nm thick Al layer on the Ge(111) substrate kept on substrate temperature $T_S = 620°C$. The deposited Al atoms form islands structures with average diameter $d = 65$ nm, as seen in Figure 4.15 a). Al NP deposition was done by Ing. Tomáš Pejchal.

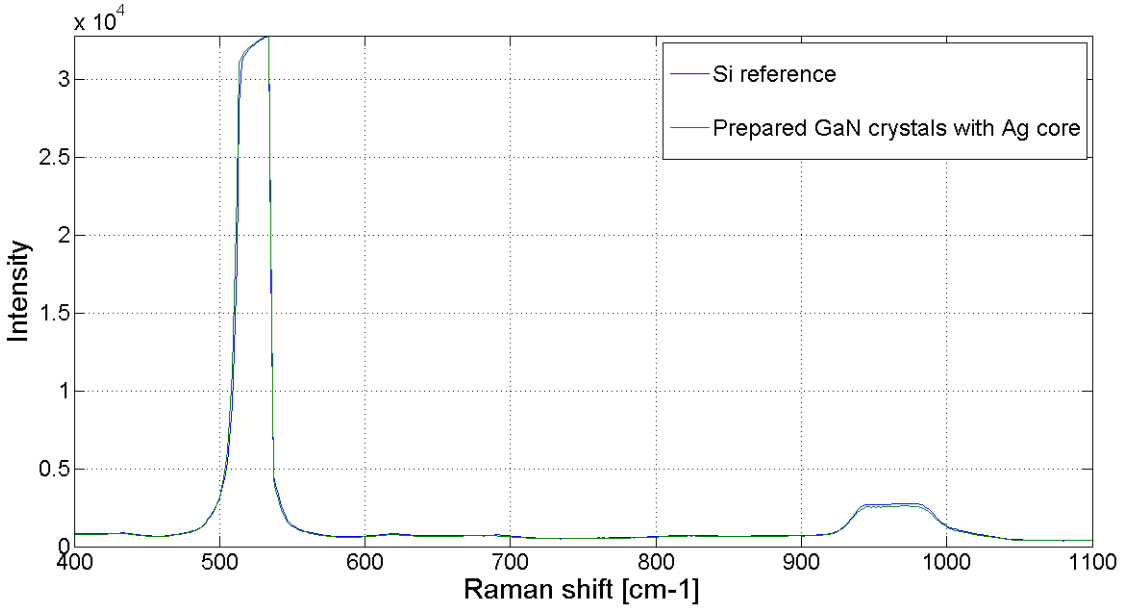

Figure 4.14: Raman spectra of prepared GaN crystals with the Ag core (green curve) and reference Si(111) substrate with Ag NPs (blue curve).

Similarly to Ag NPs, the next step was Ga deposition. The Ge(111) sample with Al NPs was annealed in UHV at temperature $T = 350°C$ for $t = 100$ min. For Ga deposition the same Ga effusion cell as in previous experiments was used. The Ga deposition was done at substrate temperature $T_S = 350°C$ for $t = 60$ min with flux $I_J = 78$ nA. The SEM image after Ga deposition (Figure 4.15 b)) shows two distinct features. By comparing the images before and after Ga deposition the bright features can be assigned to Ga droplets on the surface. The Ga droplets do not seem to contain an Al NP and rather stay apart from Al NPs. To prepare GaN crystals with the Al core we need to prepare Ga droplets containing one Al NP. To achieve this, deposition parameters in further research has to be optimized.

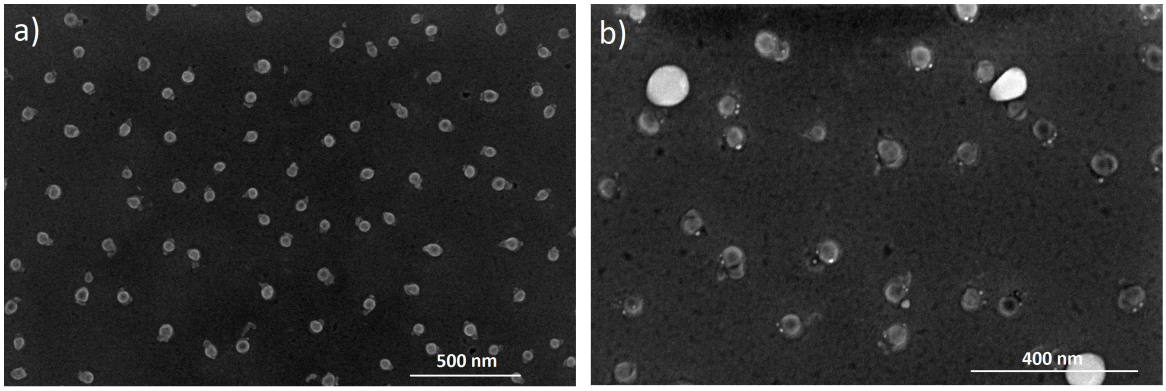

Figure 4.15: a) SEM image of Al NPs on the Ge(111) substrate prepared by Ing. Tomáš Pejchal. b) SEM image of Al NPs on the Ge(111) substrate after Ga deposition. The bright features are Ga droplets. Images taken in CEITEC on FEI Verios 460L.

5 SUMMARY

The goal of this work was to prepare GaN crystals with a metal core and to measure the basic properties of prepared structures. The preparation of GaN crystals with a metal core consists of three steps: 1. Metal NPs deposition, 2. Ga deposition, 3. Post-nitridation.

In the theoretical part of this work I have discussed the basic principles of epitaxially grown thin films. In the next chapter properties and applications of GaN were introduced. Further, the advantages and disadvantages of selected substrates used for GaN deposition were discussed, and the preparation methods of bulk, thin films, and nanostructures of GaN were listed. Within the MBE method the principle of a Ga effusion cell, electron-impact ion source, and modified IBAD-MBE growth method were described in more detail.

In the third chapter the properties and the deposition process of metal NPs from colloidal solution were introduced. Further, the basic principles of photoluminescence and the possibility to enhance photoluminescence by introducing metal NPs to a GaN structure were discussed.

The experimental section was divided into three parts according to the preparation steps of GaN crystals with the metal core. In the first step the process of Ag NPs deposition from a colloidal solution was optimized. Suitable Ag NPs deposition on the Si(111) substrate was achieved after immersing the substrate for $t = 20$ min in the 2.5 mM HCl modified colloidal solution.

In the second step after Ga deposition SEM/EDX and SAM/AES measurements have shown that the Ag NPs are not stable during the Ga deposition. The Ag-Ga phase diagram shows that almost 15% of Ag dissolve in Ga. This was undesirable, and therefore several approaches were proposed to eliminate the Ag dissolution in Ga. A successful passivation of Ag NPs was achieved after leaving the annealed Ag NPs in the air for $t = 19$ hours. A thin silver oxide layer formed on Ag NPs protects these nanoparticles from dissolution during the Ga deposition.

After successful deposition of Ga droplets, i.e. without influencing Ag NPs, the formation of GaN can occur. Two experiments were done, varying in the deposition time. XPS spectra confirmed that $\sim 80\%$ of Ga on the surface was transformed into GaN. We believe that in the SEM images Ag NPs can be seen (bright features), proving that GaN crystals with Ag core were prepared. The 55° tilted SEM images reveal that some small Ga droplets were transformed into a rod/wire structure. The origin and composition of these structures is uncertain and it will be a topic for further study.

GaN crystals prepared with the Ag core performed a strong NBE luminescence peak positioned at $\lambda = 365$ nm. Surprisingly, no YL peak coupled with defects was

seen in the spectra. Our structures were also examined by the Raman spectroscopy for potential SERS effects. The SERS effect in our structures was not proven.

Attempts to prepare GaN crystals with the Al core were made. After depositing Ga on Al NPs on the Ge(111) substrate the Ga atoms formed Ga droplets apart from Al NPs.

BIBLIOGRAPHY

[1] Akasaki, I., Amano, H., and Nakamura, S.: *The Nobel Prize in Physics 2014*. The Royal Swedish Academy of Science, 2014. [online] Link: `https://www.nobelprize.org/nobel_prizes/physics/laureates/2014/press.html`.

[2] Jang, L. W., Jeon, D. W., Sahoo, T., Polyakov, A. Y., Saravanakumar, B., Yu, Y. T., Cho, Y. H., Yang, J. K., and Lee I. H.: *Energy coupling processes in InGaN/GaN nanopillar light emitting diodes embedded with Ag and Ag/SiO_2 nanoparticles*, J. Matter. Chem., 22, p. 21749-21753, 2012.

[3] Wandelt, K.: *Surface and Interface Science*, Wiley-VCH, 2015. ISBN: 978-3-527-41158-0.

[4] Herman, M. A. and Sitter, H.: *Molecular Beam Epitaxy*, Springer-Verlag Berlin Heidelberg, 1996. ISBN: 978-3-642-80060-3.

[5] Seshan, K.: *Handbook of thin-film deposition precesses and techniques: Principles, Methods, Equipment and Applications*, William Andrew publishing Norwich, New York, USA, 2002. ISBN: 0-8155-1442-5.

[6] Ohring, M.: *The Materials Science of Thin Films*, Academic Press,San Diego, 1992. ISBN 0-125-24975-6.

[7] Magnfalt, D.: *Fundamental processes in thin film growth: The origin of compressive stress and the dynamics of the early growth stages*. [Dissertation], Linköping University, Sweden, 2014. Link: `https://liu.diva-portal.org/smash/get/diva2:710286/FULLTEXT01.pdf`.

[8] Venables, J. A.: *Introduction to Surface and Thin Film Processes*, Cambridge: Cambridge University Press, 2000. ISBN 0-521-62460-6.

[9] Ghosh, D. C. and Gupta, K.: *A new scale of electronegativity of 54 elements of periodic table based on polarizability of atoms*, Journal of Theoretical and Computational Chemistry, 5, p. 895-911, 2006.

[10] Yao, T. and Hong, S.-K.: *Oxide and Nitride Semiconductors Processing, Properties, and Applications*, Springer, p. 1-17, 2009. ISBN: 978-3-540-88846-8.

[11] Kirilyuk, V.: *Optical characterization of gallium nitride*, PhD thesis, University of Nijmegen, Imperial College Press, 2002.

[12] Suzuki, M., Uenoyama, T., and Yanase, A.: *First-principles calculations of effective-mass parameters of AlN and GaN*, Phys. Rev. B., 52, p. 8132-8139, 1995.

[13] Paisley, M. J., Sitar, Z., Posthill, J. B., and Davis, R., F.: *Growth of cubic phase gallium nitride by modified molecular-beam epitaxy*, Journal of Vacuum Science and Technology A: Vacuum, Surfaces, and Films, 7, p. 701, 2016.

[14] Shur, M. S.: *GaN-based Electronic Devices*, p. 61.-85., [online] Link: `http://ieeexplore.ieee.org/stamp/stamp.jsp?arnumber=1504293`.

[15] Liu, L. and Edgar, J. H.: *Substrates for gallium nitride epitaxy*, Materials Science and Engineering R, 37, p. 61-127, 2002.

[16] Ke, X., Jian-Feng, W., and Guo-Qiang, R.: *Progress in bulk GaN growth*, Chin. Phys. B, 24, (066105), 2015.

[17] Lidow, A., Strydom, J., Rooij, M., and Reusch, D.: *GaN Transistors for Efficient Power Conversion*, Wiley, 2014. ISBN: 978-1-118-84476-2.

[18] Takahashi, K., Yoshikawa, A., and Sandhu, A.: *Wide Bandgap Semiconductors*, Springer, Heidelberg, 2007. ISBN 978-3-540-47234-6

[19] Bougrov, V., Levinsthein, M. E., Rumyanstev, S. L., and Zubrilov, A.: *Properties of Advanced Semiconductor Materials GaN, AlN, InN, BN, SiC, SiGe*, Inc., New York, p. 1-30, 2001.

[20] Lambrecht, W. R. and Segall, B.: *Anomalous band-gap behavior and phase stability of c-BN-diamond alloys*, Phys. Rev. B, 47, p. 9289-9296, 1993.

[21] Lu, H. and Meng, X.: *Correlation between band gap, dielectric constant, Young's modulus and melting temperature of GaN nanocrystals and their size and shape dependences*, Sci. Rep., 5, 2015.

[22] Leinen, H., Glassner, D., Metcalf, H., Wynands, R., Haubrich, D., and Meschede, D.: *GaN blue diode lasers: a spectroscopist's view*, Appl. Phys. B, 70, p. 567–571, 2000.

[23] Reusch, D. and Strydom, J.: *Effectively paralleling gallium nitride transistors for high current and high frequency applications*, IEEE Conference Publications, p. 745-751, 2015.

[24] Wang, X. and Yoshikawa, A.: *Molecular beam epitaxy growth of GaN, AlN and InN*, Progress in Crystal Growth and Characterization of Materials, 48/49, p. 42-103, 2004.

[25] Doppalapudi, D., Iliopoulus, E., Basu, S. N., and Moustakas, T. D.: *Epitaxial growth of gallium nitride thin films on A-plane sapphire by molecular beam epitaxy*, J. Appl. Phys., 85, p. 3582-3589, 1999.

[26] Lieten, R. R., Degroote, S., Cheng, K., Leys, M., Kuijk, M., and Borghs, G.: *Growth of GaN on Ge(111) by molecular beam epitaxy*, Appl. Phys. Lett., 89, 252118, 2006.

[27] Lieten, R. R., Degroote, S., Leys, M., and Borghs, G.: *Suppression of domain formation in GaN layers grown on Ge(111)*, Journal of Crystal Growth, 311, p. 1306-1310, 2009.

[28] Denis, A., Goglio, G., and Demazeau, G.: *Gallium nitride bulk crystal growth process: A review*, Materials Science and Engineering R, 50, p. 167-194, 2006.

[29] Bockowski, M.: *High nitrogen pressure solution growth of GaN*, Jpn. J. Appl. Phys. 53, 100203, 2014.

[30] Ehrentraut, D., Meissner, E., and Bockowski, M.: *Technology of Gallium Nitride Crystal Growth*, Springer, 2010. ISBN: 978-3-642-04828-9.

[31] Kawamura, F., Morishita, M., Tanpo, M., Imade, M., Yoshimura, M., Kitaoka, Y., Mori, Y., and Sasaki, T.: *Effect of carbon additive on increases in the growth rate of 2 in GaN single crystals in the Na flux method*, j. Crys. G., 310, p. 3946-3949, 2008.

[32] Maruska, H. P. and Tietjen, J. J.: *The preparation and properties of Vapor-deposited single-crystalline GaN*, Appl. Phys. Lett., 15, p. 327-329, 1969.

[33] Zhang, W. and Meyer, B. K.: *Growth of GaN quasi-substrates by hydride vapor phase epitaxy*, Phys. Stat. Sol., 0, p. 1571-1582, 2003.

[34] Mares, P.: *The deposition of Ga and GaN nanostructures on silicon and graphene substrate*. [Master thesis], Brno University of Technolofy, 2014.

[35] Gerard, F.: *Advances in Condensed Matter and Materials Research*, Nova Science Publishers, Inc., 2004. ISBN: 1-59033-801-4.

[36] Herman, M.A., Richter, W., and Sitter, H.: *Epitaxy: Physical Principles and Technical Implementation*, Springer, 2004. ISBN: 978-3-642-08737-0.

[37] Mach, J.: *Development and application of an UHV equipment for deposition of thin films (atomic and ion system)*. [dizertation], Brno University of Technology, 2009.

[38] Almlof, J., Deleeuw, B. J., Taylor, P. R., Bauschlicher, C. W., and Siegbanh, P.: *The dissociation energy of* N_2, International Journal of Quantum Chemistry, 36, p. 345-354, 1989.

[39] Mach. J., Samoril, T., Voborny, S., Kolibal, M., Zlamal, J., Spousta, J., Dittrichova, L., and Sikola, T.: *An ultra-low energy (30–200 eV) ion-atomic beam source for ion-beam-assisted deposition in ultrahigh vacuum*, Rev. Sci. Instrum., 82, 083302, 2011.

[40] Voborny, S., Kolibal, M., Mach, J., Cechal, J., Babor, P., Prusa, S., Spousta, J., and Sikola, T.: *Deposition and in-situ characterization of ultra-thin films*, Thin Solids Films, 459, p. 17-22, 2004.

[41] Gerlach, J. W., Ivanov, T., Neumann, L., Hoche, Th. Hirsch, D., and Rauschenbach, B.: *Epitaxial GaN films by hyperthermal ion-beam nitridation of Ga droplets*, J. Appl. Phys., 111, 113521, 2012.

[42] Choi, H.-J.: *Semiconductor Nanostructures for Optoelectronic Devices*. Springer-Verlag Berlin Heildelberg, 2012. [online] Link: `file:///C:/Users/Kluci/Downloads/9783642224799-c1.pdf`

[43] Oh, E., Lee, B. W., Shim, S., Lee, K.-Y., Choi, H.-J., Son, B. H., Ahn, Y. H., and Dang, L. S.: *Platinum-Assisted Vapor-Liquid-Solid Growth of GaN Nanowires and Their Properties*, Journal of the Korean Physical Society, 56,p. 100-103, 2010.

[44] Knotek, M.: *Selective growth of GaN nanostructures on silicon substrates*. [Master thesis], Brno University of Technology, 2015.

[45] Li, S. and Waag, A.: *GaN based nanorods for solid state lighting*, J. Appl. Phys., 111, 071101, 2012.

[46] Debnath, R. K., Meijers, R., Richter, T., Stoica, T., Calarco, R., and Luth, H.: *Mechanism of molecular beam epitaxy growth of GaN nanowires on Si(111)*, Appl. Phys. Lett., 90, 123117, 2007.

[47] Bertness, K. A., Roshko, A., Mansfield, L. M., Harvey, T. E., and Sanford, N. A.: *Mechanism for spontaneous growth of GaN nanowires with molecular beam epitaxy*, Journal of Crystal Growth, 310, p.3154–3158, 2008.

[48] Tessarek, C., Heilmann, M., Butzen, E., Haab, A., Hardtdegen, H., Diekec, C., Spiecker, E., and Christiansen, S.: *the Role of Si during the Growth of GaN Mirco- and Nanorods*, Cryst. Growth Des., 14, p.1486-1492, 2014.

[49] Bertness, K. A., Roshko, A., Sanford, N. A., Barker, J. M., and Davydov, A. V.: *Spontaneously grown GaN and AlGaN nanowires*, Journal of Crystal Growth, 287, p.522–527, 2006.

[50] Faraday, M.: *The Bakerian lecture:experimental relations of gold (and other metals) to light*, Philosofical Transactions of the Royal Society of London, 147, p.159, 1847.

[51] Mody, V. V., Siwale, R., Singh, A., and Mody, H. R.: *Introduction to metallic nanoparticles*, J. Pharm. Bioallied Sci., 2, p. 282-289, 2010.

[52] Barth, J. V., Costantini, G., and Kern, K.: *Review Article Engineering atomic and molecular nanostructures at surfaces*. Nature, 437, p. 671-679, 2005.

[53] Rai, M.: *Green Biosynthesis of Nanoparticles: Mechanisms and Applications*. Berforts Information Press Ltd., p. 53-56, 2013. ISBN: 978-1-78064-223-9.

[54] Lee, Z., *et al.*: *Direct Imaging of Soft-Hard Interfaces Enabled by Graphene,* Nano Lett., 9, p. 3365-3369, 2009.

[55] Ligmajer, F.: *Ordered and Disordered Arrays of Colloidal Nanoparticles for Biomolecule Detection*, [diplomová práce], 2013.

[56] Pashley, R. and Karaman, M.: *Applied Colloid and surface Chemistry.* Wiley, p. 109, 2004.

[57] Czech and Slovak Crystallographic Association, *Zeta potenciál zeta*, (vid. 21.1.2017), dostupné z: `https://www.xray.cz/kfkl-osa/eng/zetasizer/zeta.htm`.

[58] Seab, T., M., Alshammari, A., S., Al-Brahim, H. a Al-Rubeaan, K., A., *Production of Silver Nanopraticles with Strong and Stable Antimicrobial Activity against Highly Pathogenic and Multidrug Resistant Bacteria*, The Scientific World Journal, 2014, p. 863-872, 2014.

[59] Kolíbal, M., Konečný, M., Ligmajer, F., Škoda, D., Vystavěl, T., Zlámal, J., Varga, P. a Šikola, T.: *Guided Assembly of Gold Colloidal Nanoparticles on Silicon Substrates Prepatterned by Charged Particle Beams*, ACSNano, 6, p. 10098-10106, 2012.

[60] Musálek, T.: *Růst polovodičových nanovláken použitím dvousložkového katalyzátoru*, [diplomová práce], 2016.

[61] Pelant, I. and Valenta, J.: *Luminiscenční spektroskopie* [Luminescence spectroscopy], Academia, Prague, 2006. ISBN: 80-200-1447-0.

[62] Garlick, G. F. J.: *Luminescence*, Springer Berlin Heidelberg, 1958. ISBN: 978-3-662-35394-3.

[63] Heiman, D.: *Photoluminescence Spectroscopy*, Northeastern University, 2004. [online] Link: `http://tns.ndhu.edu.tw/~clcheng/class-94/bio-phy94/Class-2-PL.pdf`.

[64] Santana G., *et al.*: *Photoluminescence Study of Gallium Nitride Thin Films Obtained by Infrared Close Space Vapor Transport*, Materials, 6, p. 1050-1060, 2013.

[65] Reshchikov, M. A.: *Evaluation of GaN by photoluminescence measurement*, Phys. Status Solidi C, 8, p. 2136-2138, 2011.

[66] Zhang, X., Kung, P., Saxler, A., Walker, D., Wang, T., and Razeghi, M.: *Photoluminescence study of GaN*, Acta Physica Polonica A, 88, p. 601-605, 1995.

[67] Hong, C. H., Pavlidis, D, Brown, S. W., and Rand, S. C.: *Photoluminescence investigation of GaN films grown by metalorganic chemical vapor deposition on (111) GaAs*, J. Appl. Phys. 77, p. 1705-1709, 1995.

[68] Cho, Ch. Y., Kwon, M. K., Lee, S. J., Han, S. H., Kang, J. W., Kang, S. E., Lee, D. Y., and Park, S. J.: *Surface plasmon-enhanced light-emitting diodes using silver nanoparticles embedded in p-GaN*, Nanotechnology, 21, 205201, 2010.

[69] Cho, Ch. Y., Kim, K. S., Lee, S. J., Kwon, M. K., Ko, H., Kim, S. T., Jung, G. Y., and Park, S. J.: *Surface plasmon-enhanced light-emitting diodes with silver nanoparticles and SiO_2 nano-disks embedded in p-GaN*, Appl. Phys. Lett., 99, 041107, 2011.

[70] Giannini, V., Fernández-Domínguez, A.I., Sonnefraud, Y., Roschuk, T., Fernández-García, R., and Maier, S.A.: *Controlling Light Localization and Light–Matter Interactions with Nanoplasmonics*, Small, 6, p. 2498–2507, 2010.

[71] Mertens, H., Koenderink, A.F., and Polman, A.: *Plasmon-enhanced luminescence near noble-metal nanospheres: comparison of exact theory and an improved Gersten and Nitzan model*, Phys. Rev. B, 76, 115123, 2007.

[72] Sharvani, S., Upadhayaya, K., Kumari, G., Narayana, C., and Shivaprasad, S. M.: *Nano-morphology induced additional surface plasmon resonance enhancement of SERS sensitivity in Ag/GaN nanowallnetwork*, Nanotechnology, 26, 465701, 2015.

[73] Nie, B., Duan, B. K., and Bohn P. W.: *Nanoporous Ag–GaN thin films prepared by metal-assisted electroless etching and deposition as three-dimensional*

substrates for surface-enhanced Raman scattering, J. Raman Spectrosc., 43, p. 1347-1353, 2012.

[74] Kneipp, K.: *Chemical Contribution to SERS Enhancement: An Experimental Study on a Series of Polymethine Dyes on Silver Nanoaggregates*, J. Phys. Chem. C, 120, p. 21076-21081, 2016.

[75] Wang, R., Liu, D., Zuo, Z., Yu, Q., Feng, Z., Liu, H., and Xu, X.: *Surfactantless photochemical growth of Ag nanostructures on GaN epitaxial films with controlled morphologies and their application for SERS*, J. Matter. Chem., 22, p. 2410-2418, 2012.

[76] Milekhin, A. G., Meijers, R., Richter, T., Calarco, R., Luth, H., Paez Sierra, B. A., and Zahn, D. R. T.: *Surface enhanced Raman scattering by GaN nanocolumns*, Phys. stat. sol. (c), 3, p. 2065-2068, 2006.

[77] Milekhin, A. G., Sveshnikova, L. L., Duda T. A., Yeryukov, N. A., Rodyakina, E. E., Gutakovskii, A. K., Batsanov, S. A., Latyshev, A. V., and Zahn, D. R. T.: *Surface-enhanced Raman spectroscopy of semiconductor nanostructures*, Physica E 75, p. 210-222, 2016.

[78] Kuball, M.: *Raman spectroscopy of GaN, AlGaN and AlN for process and growth monitoring/control*, Surf. Interface Anal., 31, p. 987–999, 2001.

[79] Sharma, B., Frontiera, R. R., Henry, A.-I., Ringe, E., and Van Duyne, R. P.: *SERS: Materials, applications, and the future*, Materials today, 15, p. 16-25, 2012.

[80] Premovic. M., Du, Y., Minic, D., Sundman, B., Zhang, C., Watson, A., Manasijevic, D., and Djordjevic, A.: *Experimental investigation and thermodynamic calculations of the Ag–Ga–Sn phase diagram*, CALPHAD: Computer Coupling of Phase Diagrams and Thermochemistry, 56, p. 215–223, 2017.

[81] Philips Lighting Holding B.V.: *Scanning Auger Microscopy (SAM/AES)*, 2016. [online] Link: `http://www.innovationlabs.philips.com/images/pdf/MaterialAnalysis/material-analysis-SAM.pdf`

[82] Prochazka, P., Mach, J., Bischoff, D., Liskova, Z., Dvorak, P., Vanatka, M., Simonet, P., Varlet, A., Hemzal, D., and Petrenec, M.: *Ultrasmooth metallic foils for growth of high quality graphene by chemical vapor deposition*, Nanotechnology, 25, 185601, 2014.

[83] Bardy, S.: *Deposition of Ga and GaN nanostructured on graphene substrate treated by atomic hydrogen.* [Master thesis], Brno University of Technolofy, 2016.

[84] Rooij, A.: *The Oxidation of Silver by Atomic Oxygen*, ESA Journal, 13, p. 363-382, 1989.

[85] Waterhouse, G. I. N., Bowmaker, G. A., and Metson, J. B.: *The thermal decomposition of silver (I, III) oxide: Acombined XRD, FT-IR and Raman spectroscopy*, Phys. Chem. Chem. Phys., 3, p. 3838-3845, 2001.